Fermi National Accelerator Laboratory

FERMILAB-Pub-83/89-THY
Oct., 1983
Submitted to Phys. Rev. D

The Ultra-High Energy Cosmic Ray Spectrum

Christopher T. Hill
Fermi National Accelerator Laboratory, P.O. Box 500
Batavia, Illinois, 60510

and

David N. Schramm
The University of Chicago, Chicago, Illinois
and
Fermi National Accelerator Laboratory

Abstract

We analyze the evolution of the ultra-high energy cosmic ray spectrum upon traversing the 2.7^{o}K microwave background with respect to pion photoproduction, pair production reactions, and cosmological effects. Our approach employs exact transport equations which manifestly conserve nucleon number and embody the laboratory details of these reactions. A spectrum enhancement appears around 6×10^{19}ev due to the "pile-up" of energy degraded nucleons, and a "dip" occurs around 10^{19}ev due to combined effects. Both of these features appear in the observational spectrum. We analyze the resulting neutrino and gamma spectra and the effects of cosmological source distributions. We present a complete model of the UHE spectrum and anisotropy in reasonable agreement with observation and which predicts an observable electron neutrino spectrum.

FERMILAB-Pub-83/89-THY
Oct., 1983

The Ultra-High Energy Cosmic Ray Spectrum

Christopher T. Hill
Fermi National Accelerator Laboratory, P.O. Box 500
Batavia, Illinois, 60510

and

David N. Schramm
The University of Chicago, Chicago, Illinois
and
Fermi National Accelerator Laboratory

Abstract

We analyze the evolution of the ultra-high energy cosmic ray spectrum upon traversing the $2.7^{o}K$ microwave background with respect to pion photoproduction, pair production reactions, and cosmological effects. Our approach employs exact transport equations which manifestly conserve nucleon number and embody the laboratory details of these reactions. A spectrum enhancement appears around $6x10^{19}$ev due to the "pile-up" of energy degraded nucleons, and a "dip" occurs around 10^{19}ev due to combined effects. Both of these features appear in the observational spectrum. We analyze the resulting neutrino and gamma spectra and the effects of cosmological source distributions. We present a complete model of the UHE spectrum and anisotropy in reasonable agreement with observation and which predicts an observable electron neutrino spectrum.

I. Introduction

Shortly after the discovery of the $2.7^{\circ}K$ microwave background radiation it was suggested that there must exist a fundamental cut-off in the ultra-high energy cosmic ray spectrum[1,2]. A nucleon of energy exceeding 10^{20}ev colliding head-on with a typical $2.7^{\circ}K$ photon comprises a system of sufficient total center of mass energy to produce pions by the photoproduction reaction. The energy loss of the nucleon is a significant fraction of the incident energy. Moreover, the pion photoproduction cross-section is quite large immediately above threshold due to resonance production, rising quickly to $\sim$500 microbarns for gamma lab energies of order .3 Gev, and settling down asymptotically to roughly $\sim$120 microbarns for energies exceeding a few Gev. Thus, if as is widely believed, the ultra-high energy cosmic rays are produced in distant extra-galactic sources, then the observed spectrum must be cut-off at an energy scale of order 10^{20}ev. In fact, if the sources are more than a few interaction lengths away, then collisions with photons in the high energy Boltzmann tail of the $2.7^{\circ}K$ photon distribution will reduce the onset of the cut-off to about 5×10^{19}ev. These are the theoretical conclusions of refs.(1,2) and subsequent treatments, however in the present paper we will find that in general there can be a dramatic departure from these conclusions.

It is widely believed that cosmic rays of energies exceeding 10^{15}ev begin to leak out of the galactic confining magnetic field. At this energy scale we encounter the so-called "knee" in the observed spectrum, which steepens from a differential index of 2.5 below 10^{15}ev to $\sim$3 above and which has been attributed to a magnetic deconfinement effect[3,4].

At 10^{15}ev the Larmor radius in the Galactic disk is $\sim$1 light year. If the motion in the galaxy was purely diffusive, this would correspond to a diffusion constant of $\sim$ 1 $(\text{lyr})^2/\text{yr}$, and the diffusion time necessary to traverse the disk width, 10^3 lyr., would be correspondingly $10^3 \sim \sqrt{\kappa t}$ or $t \sim 10^6$yr. Of course, the motion will not be purely diffusive since cosmic rays can migrate along field lines with a velocity of order c. Indeed, since $\kappa \propto E$, the above argument would predict a diffusion time $t \propto E^{-1}$, which grossly overestimates the known age of lower energy cosmic rays because the observed flux will be proportional to the trapping time in the galaxy. A trapping time $t \propto E^{-1}$ would require an extremely flat injection spectrum $j(E) \propto E^{-1.5}$. Nonetheless, it is probable that the trapping time is mildly energy dependent at $E \rightarrow 10^{15}$ev and for $E > 10^{15}$ev, becomes rapidly so, becoming quickly small compared to an inverse replenishment rate. Below 10^{15}ev, we might expect a roughly scale invariant injection spectrum $\sim 1/E^2$ and a trapping time falling like $1/\sqrt{E}$, to account for the observed $1/E^{2.5}$. Scale invariant spectra are known to occur in several astrophysical settings, and would seem to be required to account for such extremes of energies as are found in cosmic rays. Indeed, we will find that a $1/E^2$ injection spectrum yields the best fit to the observed structure above 10^{18}ev. An important corollary of the leakage model of the knee is the observation of an increasing (Fe) abundance, which is expected if lighter nucleons leak out at lower energies, and if Fe is found in low ionization states (small e/m).

An observer inside of the galaxy sees, therefore, a spectrum behaving like $j_o(E)t(E) \sim 1/E^{2.5}$, steepening to $1/E^{3.0}$ for $E > 10^{15}$ev. If we discount the cosmic rays produced in other galaxies, we might

expect that the steep part of the spectrum continues until a "line of sight" or "prompt" component is reached from local galactic events. This might be argued to be the source of the "ankle" at energies above 10^{19}ev. The difficulty here is that the reported corollary anisotropy is directed normal to the galactic plane (in the general direction of the Virgo cluster)[5]. One might argue that the iron-rich spectrum could be steered by the galactic B-field to produce such an effect. However, this mechanism may be difficult to implement in the known geometry of the galactic B-field. Furthermore, the prompt component of the spectrum should not be iron rich, since it is not subject to the trapping time effect, and it should contain mostly protons and even neutrons. Thus the anisotropy becomes hard to understand; in fact the absence of a pin-point image of the source in the general direction of the galactic plane would be expected.

For an imaginary observer outside of the galaxy the situation is drastically different. The trapping-integration time is now effectively replaced by T_H, the Hubble time (neglecting for the moment loss effects due to redshift, pairproduction, etc.). The observer will see essentially the leakage spectrum summed over all sources, integrated over the entire history of the Universe. For an observer sitting inside of the galaxy, this cosmological contribution will also be present and we must inquire as to how its strenghth compares to that of the local sources. We expect, crudely, that the local flux is of order $1/R_G^2$, where R_G is the galactic length scale, 10^4lyr. The cosmological flux is roughly of order R_H/R_{IG}^3, where R_{IG} is the intergalactic scale $\sim 10^6$lyr, and R_H is the Hubble scale 10^{10}lyr. With these scales we see that the two fluxes are of the same order, 10^{-8}. Thus, we expect that there will

occur some energy scale, E_c, at which the local spectrum becomes comparable to or less than the cosmological component. We shall refer to E_c as the "cross-over" energy, and the above estimate suggests that cross-over must occur near the knee in the spectrum $\sim 10^{(15 \text{ to } 16)}$ev. Of course, the existence of the cross-over depends upon the extent to which the local spectrum steepens by leakage, the steepening effects which may be present in the cosmological spectrum, and the overall normalizations. In fact, we shall find that there must exist some steepening of the cosmological spectrum due to cosmological redshift effects, a point originally emphasized by Hillas[7]. We emphasize that it is not known definitively whether the cosmic rays above 10^{15}ev are local, extragalactic or both. One of our objective presently is to improve substantially the predictions of the cosmological model.

It is then natural to associate the "ankle" structure with either the cross-over energy, or with the presence of a particulary bright extragalactic, though relatively nearby source, superimposed on a cosmological diffuse background, or both. This then fixes the normalization of the extragalactic component, and allows us to make quantitative estimates of the neutrino yields, and spectrum structure as arise by photoproduction.

Such mechanisms for the spectrum above the "knee" have been previously discussed[4,7,8,9]. Hillas[7] has argued that the structure of the spectrum between 10^{15}ev and 10^{19}ev can be understood as a cosmological evolution due to redshift effects from sources most active at large redshift, e.g. $z > 30$ to the present. Blumenthal[9] has done a quantitative analysis of the effects of pair production interactions (e^+e^- pair creation on nucleons by 2.7^{o}K photons with higher energies at

large redshift) in a Hillas model and finds a reasonable agreement with a $1/E^3$ oberved spectrum up to 10^{19}ev by assuming a flatter $1/E^{2.5}$ injection spectrum, increasing activity proportional to $(1+z)^4$, and integrating back to $z \sim 15$ to 50 (There is even a slight vestige of a flattening in Blumenthal's spectrum at 10^{19}ev). These analyses have, however, failed to describe the ankle structure due to the treatment of photomeson production. These analyses also implicitly assume the cross-over energy to be about 10^{16}ev.

However, in Section VI we will show that the occurance of the general ankle structure in models with $1/E^{2.0\pm.5}$ injection spectra are in good agreement with observation when the spectrum evolution is properly treated. We also require an assumption of proximity to the Virgo cluster, relative to the nearest typical diffuse sources, in order to accomodate the anisotropy and events reported above 10^{20}ev. We will obtain an unambiguous prediction for the neutrino and photon spectra, which should be experimentally verifiable.

A new feature which emerges in our analysis and which has not been previously discussed in the literature is the appearance of a "dip" in E^3dN/dE at about 10^{19}ev. This dip appears in the published data and is statistically significant. We feel it lends potentially strong support to the analysis presented here and to the idea of long range propagation ($>$ 100 Mpc.).

Below 10^{19}ev the spectrum shows little anisotropy while above this energy an impressive anisotropy has been reported[4,5]. This has been associated with the Virgo cluster as the source of the cosmic rays at this energy[4,8,10]. Furthermore, if nucleon sources are within our galaxy at these energies we would expect the observed cosmic rays to

have traveled essentially by line of sight, due to the relatively long Larmor radius at 10^{20}ev (about 10^4 light years) and the comparatively short coherence length of the galactic B-field (about 300 light-years; any estimate of the dispersion of arrival times and directions by galactic B-fields that neglects the coherence length of the field will be a gross overestimate.) If D is the distance of a source, R_L the Larmor steering radius at any given point in space and R_C the coherence length of the B-field, then the expected dispersion in arrival directions (in radians) is of order $(DR_C/R_L^2)^{1/2}$, and for $D=10^5$light years, R_C=300 light years, and $R_L=10^4$ light years, we obtain an angular dispersion of order .5 radians, which would seem to imply a much larger anisotropy than is observed (this estimate pertains, e.g., to models which posit a supernova explosion on the far side of the galaxy[11] and argue a reasonable arrival time dispersion, but may be neglecting the finite coherence length of the galactic B-field. Closer sources will produce less dispersion and should be essentially pin-point.) It is therefore difficult to maintain intra-galactic source models with essentially line-of-sight propagation in view of the current data on arrival directions, though we believe that it is extremely useful to formulate statistical variables with which the celestial sphere angular distribution information can be quantified. In principle the question of local sources can be settled with a decade's worth of increase in data and a study of arrival directional correlations. Furthermore, such studies for the very highest energy cosmic rays (presumably associated with a non-diffuse, "local" source such as the VIirgo supercluster, e.g. see section VI) can in principle give information on the magnitude of the intergalactic magnetic field.

If the spectrum above 10^{19}ev is extragalactic in origin then it is predominantly composed of nucleons. Nuclei are expected to have substantially broken apart by photoreactions with starlight and the $2.7^{o}K$ background photons[1,12]. We remark that even free neutrons with energy in the range 10^{19}ev to 10^{20}ev can travel distances of order (few) Mpc before beta-decay due to time dilation. Photomeson production reactions will involve neutrons, and the appropriate averaging over isospin must be included. We shall thus approximate the ultra-high energy cosmic rays as an average over nucleons (and antinucleons) in the evolution of the spectrum. The production of $e^{+}e^{-}$ pairs is extremely important and is also considered. Though the cross-section for this process is roughly 3 to 4 orders of magnitude larger than that of photomeson production, the energy loss per nucleon is correspondingly 6 orders of magnitude smaller. This is an extremely important effect cosmologically for nucleons that have traversed a distance of order a tenth of the present horizon radius (this need be only the total path length traversed, and need not be the total range of the particle due to magnetic localization on a supercluster scale). We shall not follow the produced $e^{+}e^{-}$ pairs which rapidly lose energy by Compton scattering on the $2.7^{o}K$ photons[13] and by synchrotron energy loss in the intergalactic magnetic field. Correspondingly, there will develop a high energy gamma component, and the appropriate transport equation describing these components must allow for the mixing of gammas to pairs and vice-versa[14]. These are extremely important potential corollary observables which should be analyzed in detail, as we have presently for the induced neutrino spectrum.

Observationally there is a controversial development in the ultra high energy cosmic ray spectrum which onsets at about $3x10^{19}$ev. Here some groups report a general flattening of the spectrum from a differential index of order 3.0 to about 2.5.[15,16] Also, there are a large number of events reported with energies exceeding 10^{20}ev.[15,16] This is seemingly very difficult to understand in terms of the conventional Greisen-Zatsepin cut-off with extragalactic sources. On the contrary, the Yakutsk group after previously claiming to have seen the effect now reports no flattening of the spectrum at these energies[17] and results generally consistent with the expectation of a cut-off. Though the reported flattening derives from significantly more data, the Yakutsk data involves greater redundancy in energy calibration. The ankle may or may not be seen by the southern hemisphere group[18]. However, Yakutsk also fails to see the dramatic anisotropy reported by the Haverah park group, and it is difficult to understand this discrepancy which is less immune to the problems of energy calibration. Furthermore, a recent comparative analysis of the electromagnetic calibration of the Haverah Park array and the Yakutsk array shows that they are generally consistent[19], compounding the mystery of the discrepancy. The resolution of this dilemma will perhaps await better statistics and more data involving greater integrated energy measurements[20]. The Fly's Eye experiment is in an excellent position to refine the data on UHE CR's since their detection method integrates the shower development, and is sensitive to $\sim$100km^2. They may also detect upward or horizontal events which might be missed entirely with a conventional array, and have already provided new limits on the presence of ultra high energy cosmic ray neutrinos. This latter

subject will be dealt with at length in the present paper and our best fit to the nucleon spectrum will predict a neutrino flux above 10^{18}ev comparable to the Fly's Eye limit above 10^{19}ev.

It is in part due to this interesting and exciting controversy that we have undertaken to reanalyze the Greisen-Zatsepin cut-off in the more reliable framework of transport equations. Given a final verdict on the observational situation, what can we hope to learn about the underlying mechanisms? Also, given the present observational situation can we begin to glimpse a complete picture of the sources, origins and evolutionary effects inherent in the UHE cosmic rays? In the present paper we argue from the vantage point of an improved evolutionary analysis that the UHE spectrum is indeed beginning to form a consistent picture.

In the present paper we will reexamine the expectations for the structure of the cosmic ray spectrum at ultra-high energies (see refs.(21,22)). Our method will differ from those of preceding authors in a significant way. Instead of the mean interaction length and energy loss approximations used in preceding analyses[23,8] we will employ statistically exact transport equations which incorporate the laboratory details of photoproduction and meson decays. An important aspect of our analysis is the explicit conservation of baryon number which leads to an "active recoil nucleon" and the collision processes are iterated until the recoil particles drop effectively below threshold to participate in further interactions. This leads to an effective multiplier in the number of secondary photons and neutrinos that are produced since one nucleon can experience several collisions in this cascade process. Also we find that, contrary to previous analyses and expectations pervading

the literature, structure at this energy scale does occur as a natural result of the photoproduction, pair production and cosmological redshift effects.

We find that an enhancement always occurs before the GZ cutoff as a consequence of the pile-up of energy degraded nucleons recoiling down from higher energies and ending up approximately below threshold to undergo further photoproduction reactions, of order 5×10^{19}ev. The shape of the enhancement is essentially "universal" in the sense that after a few interaction lengths it is very weakly dependent upon the input spectrum shape, but does depend strongly upon the input spectrum normalization. This is remniscent of a "fixed point" behavior. In fact, we find that the spectrum above 10^{18}ev can be understood completely in terms of an injection spectrum of order $1/E^{2.0 \pm .5}$ which is steepened by the various cumulative effects and interactions into a $1/E^3$ form up to 3×10^{19}ev, and we can accomodate, by including a "local" or exceptionally bright source, e.g. the Virgo supercluster, a large "ankle" structure extending up to 10^{20}ev. This model can incorporate, but does not require, a Hillas-Blumenthal model for the spectrum from 10^{15}ev to $\sim 10^{18}$ev or a magnetic confinement-leakage model. In spirit this is a model quite similar to that discussed previously by Giler, Strong, Wdowczyk and Wolfendale[8], but differs substantially in details and results.

This model leads to an unambiguous prediction for the neutrino spectrum. In particular, even though we consider arbitrary injection indices and bright phase exponents in treating the cosmological source sums we find that the UHE neutrino spectrum always has a slope equal to the observed CR slope plus 1/2. Other features of the neutrino spectrum

emerge which contain detailed information about the "bright phase".

It should be emphasized that the physics of these reactions is completely well known, and we are simply boosting to the frame containing the incident cosmic ray nucleon of energy 10^{20}ev. In preceding analyses the shape of the spectrum above tha GZ cut-off has been analyzed in only an approximate way. Stecker[23] following the original suggestion of Greisen and Zatsepin first examined the kinematics and estimated the mean energy loss attenuation length. He has also studied the corollary phenomena of photon and neutrino production in an approximate way. Others have essentially followed Stecker's original analysis with various assumptions about sources and magnetic localization effects[8]. The approximations inherent in these analyses are essentially correct at high energies for cosmic rays traversing several or more interaction lengths. In the case of energies near the threshold and distances of order the interaction length there are certain deficiencies which arise because one neglects the recoil proton (thus not conserving baryon number) and the mean energy loss approximation breaks down where the inelasticity is rapidly varying as it is near threshold. Also, in estimating the normalization of the secondary spectrum there are important corrections (possibly as large as factors of ten) due to the active recoil nucleons. Furthermore, the pair production effects do no "commute" with the photomeson effects (the two effects are not simply additive and must be evolved simultaneously; a nucleon could, for example, lose all of it's energy by pair production alone, but it preferentially loses it's highest energies by photomeson effects, then by pair production below meson threshold). We shall briefly discuss these approximations in the next section.

The important phenomena of secondary photons and neutrinos have been proposed and analyzed by previous authors, most noteably Stecker[23]. However, these analyses again neglect the recoil proton that emerges from the initial collision, while retaining most of the incident energy and which can initiate subsequent collisions. Thus, the spectrum of produced secondaries has a normalization which is related to the pile-up normalization, but is significantly larger than that obtained previously. We will also find that our numerical evolution leads to a smaller cut-off energy in the neutrino and photon spectra than those obtained previously. We find an effective cut-off of order 2×10^{19}ev. We will obtain a non-cosmologically sensitive lower limit of about $1/km^2yr\ sr$ integrated neutrino flux above 10^{18}ev, and results roughly 100x greater with reasonable bright phase models. These latter results approach detectability in the Fly's Eye within a factor of 10 to 100. The prediction depends only upon the assumption of increasing cosmic ray activity back to redshifts greater than ~3 and that the UHE cosmic rays are extragalactic nucleons. Measuring the neutrino spectrum to lower energies than 10^{18}ev would determine the redshift of maximum CR luminosity. Thus, the prospect of a new neutrino astronomy opening up is extremely exciting.

Our paper is organized as follows. We begin in Section II with a brief estimate of the size of the effect and the secondary particle spectra. In Section III we construct the spectrum evolution transport equation and show the limits of validity of preceding analyses. We then introduce some rescaled variables that conveniently describe the kinematics in the cosmic ray laboratory frame (CRLF) and which are employed in our numerical integration routine. We briefly review

photoproduction data at low energies and describe some fits which we employ in our analysis. In the CRLF we obtain convenient parameterizations of the recoil nucleon and produced pion energy spectra in terms of our scaling variables. We briefly describe our numerical integration routine, COSEV. In section IV we discuss in detail the cosmological effects and develop a general formalism. We discuss here the somewhat nontrivial question of normalization of the diffuse relative to the local components of the nucleon and neutrino spectra. In Section V we present the results of several numerical analyses for various assumed input spectra. We consider point-like and cosmological source distributions, for which the pair production process (e^+e^- pair production) plays an important role. In Section VI we present a complete model of the UHE cosmic ray spectrum which appears to be in good agreement with the observational data. Upon first reading we might suggest that one skip directly to Sections V. and VI. We present a brief summary and conclusions in section VII.

II. A Brief Pre-Analysis

One may consider the mean energy loss of a proton of energy E interacting with a photon of typical energy, $2.7^{o}K$, undergoing photoproduction in the reaction, $\gamma N \rightarrow \pi N$. Laboratory angular distributions can be boosted to the appropriate frame for this process to obtain the recoil energy distribution, $d\sigma'(E',E)/dE'$ where E' is the recoil energy, and E the incident nucleon energy (in the CRLF the transverse lab momentum is boosted completely forward and becomes

irrelevant; the problem is effectively one dimensional as is well known). The average rms energy loss is then:

$$\Delta E \sim \left\{ \int (E - E')^2 \frac{d\sigma}{dE'}(E, E')\, dE' \right\}^{1/2} \qquad (1)$$

The resulting energy loss rate can then be estimated:

$$E^{-1}\, \partial E/\partial x \sim -\Delta E (\xi E)^{-1} \equiv -K(E) \qquad (2)$$

where ξ is the interaction length $\xi^{-1} = \langle \rho_{3K} \sigma_{\gamma N} \rangle$.

Knowing K(E) the spectrum attenuation with range is usually estimated by writing:

$$\begin{aligned} dI(E,x)/dx &\cong (\partial E/\partial x)(\partial I(E,x)/\partial E) \\ &= -K(E)\, E(\partial I(E,x)/\partial E) \end{aligned} \qquad (3)$$

where I(E,x) is the integrated spectrum above energy E at range x. Assuming a factorized solution (which will generally not be the case near threshold): $I(E,x)=f(x)E^{-\gamma}$, one finds $df/dx=-K(E)(\gamma-1)f(x)$ or:

$$f(x) = f_o \exp(-K(E)(\gamma - 1)x) \qquad (4)$$

Clearly the factorized solution is not the most general, nor is it even valid if $\partial K(E)/\partial E \neq 0$. Essentially the recoil nucleon is neglected in the collision even though the inelasticity is generally small.

The main difficulty with this approach lies in the fact that it does not take care of the transport of nucleons down from energy E to $E' < E$, to $E'' < E'$, etc., through successive collisions with the background photons. At an energy below the threshold we can have no net loss of nucleons, but we can (and generally will) have a pile-up of nucleons that have recoiled down from energies above threshold. This pile up of "deactivated" nucleons may be observable, and may indeed correlate with the observation of structure in the spectrum in this energy range.

We shall first present a heuristic argument to demonstrate the pile-up phenomenon and which will lead to a quick estimate of it's magnitude. Consider only multi-pion photoproduction, ignoring nucleon pair production. We shall assume a primary nucleon spectrum at production (or after leaving the production neighborhood) of the form $dN/dE = c/E^{\gamma}$. Assume a collision with a single photon of 4-momentum $(E_\gamma, E_\gamma, 0, 0)$ by a nucleon of 4-momentum $(E_p, -p_p, 0, 0)$. The threshold energy to produce a single pion is $E_t \sim m_p m_\pi / 2E_\gamma + O(m_\pi / m_p)$. Furthermore, in this frame the energy of the least energetic or slowest

nucleon emerging from the collision $\gamma + N \rightarrow N + X$ occurs when M_X is smallest and the nucleon and X-3-momenta are collinear and in the direction of the incident nucleon (there can never be a backward hadron, of course, which may be seen by boosting from the cm system). For incident nucleon energy E_t we have for E_s, the energy of the slowest nucleon: $E_s \sim E_t(1-m_\pi/m_p)$. Thus, near threshold $\Delta E \sim E_t(m_\pi/m_p)$. Thus, after many collisions with microwave photons the spectrum should degrade with all nucleons of initial energy $E_o > E_t$ piling up into the window $E_s < E < E_t$. Of course, this narrow window will be smeared by the Boltzmann distribution in photon energies and the peak will correspondingly be diminished. We thus see that the total number of nucleons with initial energy exceeding E_t is obtained from the assumed input spectrum:

$$\eta(E > E_t) = \frac{C}{(\gamma - 1)}\left[E_t^{-\gamma+1} - E_c^{-\gamma+1} \right] \qquad (5)$$

where E_c is a cut-off energy and $E_c >> E_t$. while the number of nucleons already in the energy window $E = E_t - E_s$ is:

$$\eta_o = c\,\Delta E/E_t^{\gamma} \sim c\,m_\pi/(m_p E_t^{\gamma-1}) \qquad (6)$$

Thus the actual accumulated excess in this energy window is:

$$\varepsilon = \left[\frac{\eta_o + \eta(E>E_t)}{\eta_o}\right] = 1 + m_p/(m_\pi(\gamma-1)) \qquad (7)$$

Assuming a primary spectral index $\gamma=3$, we see that this excess amounts to approximately $\varepsilon=4.32$, while for $\gamma=1.5$ (corresponding to a real flattening in the primary spectrum due perhaps to the onset of some new physics) we obtain $\varepsilon=14.32$. The observed flattening would seem to require an effect on the order of the latter result (the actual excess is of order a factor of 3, but extends over an energy range about 5 times the width of this window, which is how we find that this spike is smeared by the Boltzmann distribution).

The above argument is crude for several reasons: (i) The actual shape of the spectrum will be determined primarily by the structure of the $\gamma N \rightarrow \pi N$ cross-section immediately above threshold (ii) the sources may not be more than a few interaction lengths away and the evolution may thus be incomplete (iii) at cosmological distances one must include the effects of pair production interactions which will widen the pile-up and reduce its peak. Since there is virtually no uncertainty in the physics of photomeson production the only unknowns are essentially (a) the exponent γ above E_t (b) the overall normalization, c, of the

primary spectrum above E_t. Given any input spectrum we can compute the resulting evolved spectrum, but of course, the time reversed procedure will not work; all that survives ultimately is the overall normalization of the input spectrum.

A typical nucleon well above threshold will cascade down in energy until it decouples, experiencing several collisions in the process. This effectively multiplies the neutrino flux by the average number of collisions. In a previous letter[22] we have given simple estimates of this effect. Given the primary spectrum of c/E^{γ} and the inelasticity of eq.(2) we may estimate the average number of collisions in which a nucleon in the spectrum participates before dropping below threshold in the pile-up[22]. One obtains:

$$\bar{n} \sim [-\ln(1 - K(E_t))]^{-1} \left\{ \int_{E_t}^{\infty} E^{-\gamma} \ln(E/E_t)\, dE \Big/ \int_{E_t}^{\infty} E^{-\gamma} dE \right\} \quad (8)$$

which for $\gamma = 3.0$ yields $\bar{n} = 2.5$ while for $\gamma = 1.5$ yields $\bar{n} = 8$. This is a measure of the amount by which the normalization is underestimated by neglecting the recoil proton in the approximation of neglecting pair production effects. When pair production effects are included, the value of $\bar{n}$ is reduced. However, the exact spectral shape of the produced neutrinos, for example, requires a careful integration of the spectrum evolution transport equations. Nonetheless, we were surprised at how accurately these results were anticipated by the relatively crude estimates of ref.(22).

III. Spectrum Evolution Dynamics

(A) The Transport Equations

The evolution with range of the differential spectrum, $dN(E,x)/dE$, is given by the integro-differential equation (the appropriate form of the Ginzburg-Syrovatsky equation[3]):

$$\partial(dN/dE)/\partial x = -\int_{\bar{E}_\gamma=0}^{\infty} \sigma_{tot}(E,\bar{E}_\gamma)\rho(\bar{E}_\gamma)\,dN/dE\,d\bar{E}_\gamma$$

$$+\int_{E_o=0}^{\infty}\int_{\bar{E}_\gamma=0}^{\infty} \partial\sigma/\partial E(E_o,E,\bar{E}_\gamma)\rho(\bar{E}_\gamma)\,dN/dE_o\,d\bar{E}_\gamma\,dE_o \qquad (9)$$

Here σ_{tot} is the total cross-section, or suitably iso-spin averaged cross-section, for the process $N + \gamma \longrightarrow N' + \pi$, as a function of the incident nucleon energy, E_N, and the photon energy and momentum. We also include other processes together with photoproduction here. It is useful to define the photon "longitudinal energy", $\bar{E}_\gamma$, by:

$$\bar{E}_\gamma \equiv \tfrac{1}{2}(E_\gamma + p_{L\gamma}) = \tfrac{1}{2}E_\gamma(1+\cos\vartheta) \qquad (10)$$

where E_γ is the photon physical energy and where $\vartheta=0$ corresponds to the case of a "head-on" collision (photon anticollinear with the incident nucleon). The utility of eq.(10) will be seen immediately below.

$d\sigma(E,E',\bar{E}_\gamma)/dE'$ is the recoil nucleon's energy distribution as a function of incident nucleon energy, photon longitudinal energy, and the recoil nucleon energy itself, E'. We shall also require the photon

longitudinal energy distribution, $\rho(\bar{E}_\gamma)$, which we obtain from the 2.7°K blackbody distribution below.

In addition to eq.(9), we have the coupled equation describing the induced pion differential spectrum:

$$\partial(dN_\pi/dE)/\partial x = \int_E^\infty d\sigma_\pi/dE\,(E_o, E, \bar{E}_\gamma)\rho(\bar{E}_\gamma)(dN/dE_o) \cdot d\bar{E}_\gamma\, dE_o \tag{11}$$

where $d\sigma_\pi(E,E',E)/dE'$ is the single particle inclusive energy distribution of a produced pion of energy E' in terms of incident nucleon and photon energies. We can neglect the transverse momentum of the produced system with impunity in this frame (in obtaining these distributions, the transverse momentum of the produced system in the lab frame is, of course, relevant, but any transverse component is boosted essentially forward in this frame; we will obtain the dominant contributions from lab angular distributions which thus include the transverse momentum). Effectively, our present problem is one-dimensional. This equation has been used by itself to estimate the produced secondary neutrino, electron and gamma spectra assuming a fixed input spectrum, $dN_p(E)/dE$. In principle, the induced neutrino spectrum is more sensitive to the original nucleon spectrum, $dN_N(0,E)/dE$, than is the observed nucleon spectrum, which is essentially $dN(\langle x\rangle,E)/dE$, where $\langle x\rangle$ is the average source range. We shall neglect the produced e^+e^- pairs for which another coupled system of equations may be introduced.

Equation (9) conserves the total number of nucleons as is readily seen by noting that:

$$\int_0^\infty d\sigma/dE'(E_o,E',\bar{E}_\gamma)\,dE' = \langle n_N\rangle \sigma_{tot}(E_o,\bar{E}_\gamma) \tag{12}$$

and:

$$\begin{aligned}\partial I/\partial x &= (\partial/\partial x)\int_{E=0}^{\infty} dE(dN_N/dE)\\ &= -\int \sigma_t(E,\bar{E}_\gamma)\rho(\bar{E}_\gamma)(dN/dE)\,dE\,d\bar{E}_\gamma \\ &\quad + \int dE_N(\partial\sigma_N/\partial E_N)(dN/dE)\,dE\,d\bar{E}_\gamma \;\propto\; (1-\langle n_N\rangle)\end{aligned} \tag{13}$$

As long as we are kinematically below the $N\bar{N}$ threshold we have $\langle n_N\rangle=1$, and total nucleon (plus antinucleon) number is conserved. Above threshold the total number will grow. Since the $N\bar{N}$ threshold begins at $E_N=2m_p^2/\bar{E}_\gamma \simeq 3\times10^{21}$ev and since above threshold the $N\bar{N}$ production rate is a small percentage of the total, and furthermore the incident spectrum is falling at least as fast as some (large) power of E, we may neglect $N\bar{N}$ production in the following.

Taken together, eq.(9) and eq.(11) conserve total energy in the absence of pair production processes:

$$E_{tot}\,\sigma_{tot}(E_o,\bar{E}_\gamma) = \int_{E_o}^{\infty} E\,(d\sigma_N/dE + d\sigma_\pi/dE)\,dE \qquad (14)$$

Furthermore, by use of eq.(9) it is possible to understand the limits of validity of the energy loss analyses of previous authors. The total energy in the nucleon spectrum above some observable energy at a range x is:

$$\mathcal{E}(E_o,x) = \int_{E_o}^{\infty} E\,(dN_N/dE\,(E,x))\,dE \qquad (15)$$

The inelasticity of a collision is defined to be:

$$\eta(E_o) = \int_{0}^{E_o} (1 - E/E_o)\,d\sigma_N/dE\,(E_o,E)\,dE\;\sigma_{tot}^{-1}(E_o) \qquad (16)$$

Using eq.(9) we may write:

$$\partial \mathcal{E}(E_o,x)/\partial x = \int E\,\hat{\sigma}_{tot}(E)(dN/dE)\,dE + \int\int E'\,d\hat{\sigma}/dE'(E,E')\,(dN/dE)\,dE\,dE'$$

$$= \int\int E\left(1-\frac{E'}{E}\right)(d\hat{\sigma}/dE')(dN/dE)\,dE\,dE'$$

$$= \int E\eta(E)\,\hat{\sigma}_{tot}(E)\,(dN/dE)\,dE \qquad (17)$$

where the carat denotes a quantity that would normally be convoluted with the 2.7°K microwave background, $\hat{f}(u) = \int f(u,\bar{E}_\gamma)\,\rho(\bar{E}_\gamma)d\bar{E}_\gamma$. Therefore, if the product, $\eta(E)\,\hat{\sigma}_{tot}(E)$ is relatively slowly varying with energy, we may pull it outside the integral in eq.(17) and arrive at the approximate energy loss equation:

$$\mathcal{E}^{-1}(E_o,x)\,\partial\mathcal{E}(E_o,x)/\partial x = -\hat{\eta}(E_o)\,\sigma_{tot}(E_o) \qquad (18)$$

which is the usual result. If the spectrum is falling like a power, $E^{-\gamma}$, we may substitute on the rhs of eq.(18), $E \sim \mathcal{E}$, which is valid when $\gamma > 1.0$. This condition must be met for the validity of the previous analyses in addition to the points considered in our introduction. However, the main shortcoming of the above approximation is the fact that $\eta(E)\,\hat{\sigma}_{tot}(E)$ is certainly not a slowly varying function of energy near threshold.

(B) Kinematics

The kinematics of pion photoproduction in the CRLF is straightforward. It is useful to introduce scaling variables. If $\beta = 1/T$ where T is the 2.7°K photon temperature, 7.5×10^{-4}ev, then we define:

$$\bar{E}_\gamma = y\beta^{-1} \qquad E_{N(\pi)} = m_p^2 \beta x_{N(\pi)} \tag{19}$$

where $\bar{E}_\gamma$ is the photon longitudinal energy, E_N is the incident nucleon energy. The recoil nucleon has energy $E_N = z_N(m_p^2\beta)$. We find that $z_N^- \leq z_N \leq z_N^+$ and :

(20)

$$z_N^\pm = x_N \left\{ \frac{2x_N y + 1 - \varepsilon^2/2}{4x_N y + 1} \pm \frac{\left((2x_N y - \varepsilon^2/2)^2 - \varepsilon^2\right)}{4x_N y + 1} \right\}$$

where $\varepsilon = m_\pi/m_N$. Furthermore the produced pion has energy $E_\pi = z_\pi (m_p^2\beta)$ where $z_\pi^- < z < z_\pi^+$ and:

$$z_\pi^{\pm} = x_N \left\{ \frac{2x_N y + 1}{4x_N y + 1} \pm \frac{\left((2x_N y - \varepsilon^2/2)^2 - \varepsilon^2\right)^{1/2}}{4x_N y + 1} \right\} \quad (21)$$

These kinematic limits are displayed in Fig.(1). We see in Fig.(1) that the pions will be kinematically less energetic than the recoil nucleons. At high energies the rapidity distribution of multipion production pushes most of the pions away from z_π^+ while the leading particle effect pushes the nucleon toward z_N^+.

In terms of y, the photon longitudinal energy distribution is:

$$\rho(y) = \frac{\eta}{2\pi^2} \beta^{-3} y^2 \int_1^\infty \left(\exp\left(\frac{zy}{2}\right) - 1\right)^{-1} z\, dz \quad (22)$$

This is straightforwardly obtained from the Boltzmann distribution:

$$\rho(y) = \eta \int \frac{d^3k}{(2\pi)^3} \delta\left(y\beta^{-1} - \tfrac{1}{2}|K|(1+\cos\vartheta)\right) \left[\frac{2}{\left(e^{\beta|K|} - 1\right)}\right] \quad (23)$$

Here η is an overall normalization. We numerically bin the y values and normalize the distribution numerically for the given binning, and we do not require the exact analytic value of η. We find from the above distribution that the mean value of y is ~ 3.2. Thus with $2.7^{\circ}K = 2.32 \times 10^{-13}$Gev, the average threshold energy defined by $z_N^+ = z_N^-$, is $x = .027$, or $\sim 9.4 \times 10^{19}$ev.

In terms of the scaling variables the transport equations become:

$$\partial/\partial r\,(dN/dz_N) = -\int \sigma_{tot}(z_N, y)\rho(y)(dN/dz_N)\,dy + \iint(\partial\sigma_{tot}/\partial z_N(z_N, z'_N, y))\rho(y)(dN/dz_{N'})dz_{N'}\,dy$$

$$\partial/\partial r\,(dN_\pi/dz_\pi) = \iint \partial\sigma_\pi/\partial z_\pi(z_\pi, z'_N, y)\,\rho(y)(dN_N/dz'_N)\,dz'_N\,dy \qquad (24)$$

(C) Photoproduction

The general features and physics of photoproductions below 3 Gev have been extensively reviewed[24] and we refer primarily to Donnachie[24], and Genzel and Pfeil[25]. In Fig.(2) we present the total cross-sections for a number of sub-processes. The gross features are similar to those of $\pi N \to N\pi$ apart from an overall normalization factor of $\sim 1/50$. Photoproduction involves a larger number of helicity and isospin degrees of freedom and entails a more involved partial wave analysis than does πN. In general, we will not be very sensitive to the rapid variations in angular distributions of produced pions or the recoil nucleon and fits to the distributions to quadratic order in $\cos(\vartheta^*)$ (ϑ^* is the cm production angle) will suffice. We have tested this sensitivity to higher terms and even to this order find only a 5% effect. Thus, relatively simple parameterizations and fits to the low energy data will suffice. This is fortunate because the data is sparse in the channel $\gamma n \to \pi^0 n$.

The Δ resonance is the most conspicuous structure at $E_{lab}\sim.3$ Gev and we see that the single produced pion is the dominant component of the total cross-section up to $E_{lab}\sim.8$ Gev. Above 1.0 Gev the single pion process becomes a smaller fraction of the total cross-section than the multi-pronged final states. The neutron and proton total cross-sections are similar, the higher resonances being more conspicuous in the proton case, and both tend asymptotically to about 120 microbarns. The neutron total cross-section may be inferred from the deuteron total cross-section.

Detailed angular distribution data and fits are available up to 1.5 Gev for single produced pions in all but the $\gamma n\to\pi^0 n$ reaction. The parameterizations are presented as series:

$$(d\sigma/d\Omega) = \sum_{n=1}^{N} a_n \cos^n\vartheta^*; \qquad \gamma p\to\pi^0 p \tag{25}$$

$$(d\sigma/d\Omega) = (1-\beta^*\cos\vartheta^*)^{-\frac{1}{2}}\sum_{n=1}^{N} a_n\cos^n\vartheta^*; \quad \gamma\begin{pmatrix}n\\p\end{pmatrix}\to\pi^{\pm}\begin{pmatrix}p\\n\end{pmatrix}$$

where ϑ^* (β^*) is the cm system pion angle (velocity). Genzel and Pfeil[25] give tables of the coefficients a_n for various energies up to N=6. In Fig.(3) we present these coefficients for the process $\gamma p\to\pi^0 p$ Shown also is our fit to the coefficients for the cases of an assumed spherically symmetric distribution, and an approximation to quadratic order in the angular distribution. In practice only the spherically symmetric component is utilized because our energy bin size causes the other components to average to zero.

In the CRLF a nucleon of incident x_N recoils into a z'_N such that $z_N^- \leq z_N \leq z_N^+$. We seek the recoil nucleon z-distribution which is related to the cm angular distribution. If we assume in the cm system that the incident and recoil nucleons have 4-momenta given respectively by $P_i = (E,p,0,0)$ and $P'_r = (E',p'\cos(\vartheta^*),p_T,0)$, then we have in the CRLF:

$$P_{incident} = (\gamma(E+\beta p), \gamma(p+\beta E, \vec{0}_\perp) \tag{26}$$

$$P_{recoil} = (\gamma(E'+\beta p'\cos\vartheta^*), \gamma(p'\cos\vartheta^* + \beta E'), \vec{p}_\perp)$$

thus:

$$z_N^\pm = \gamma\beta^{-1}m_p^2\,(E' \pm \beta p')$$

$$dz_N = d(\gamma E'(1+\cos\vartheta^*)) = \gamma E' d\cos\vartheta^* = \tfrac{1}{2}(z_N^+ - z_N^-)\,d\cos\vartheta^*$$

$$\cos\vartheta^* = (2z_N - (z_N^+ + z_N^-))/(z_N^+ - z_N^-) \tag{27}$$

Thus the parameterization becomes:

$$(d\sigma/dz_N) = \sum_{n=1}^{N} a_n \left(\frac{2}{z_N^+ - z_N^-}\right)\left(\frac{2z_N - z_N^+ + z_N^-}{z_N^+ - z_N^-}\right)^n \tag{28}$$

or more conveniently:

$$d\sigma_{N(\pi)}/dz_{N(\pi)} = \sum_{n=1}^{N} b_n^{N(\pi)} \left(\frac{z - z^{(-)}_{N(\pi)}}{z^{(+)}_{N(\pi)} - z^{(-)}_{N(\pi)}} \right)^n \left(\frac{1}{z^{(+)}_{N(\pi)} - z^{(-)}_{N(\pi)}} \right) \qquad (29)$$

where the b_n are now linearly related to the a_n and where $N(\pi)$ denotes the nucleon (pion) case. Though this parametrization generalizes to include any degree of angular component and can incorporate the distributions of multipion final states, in practice we can safely ignore all but the n=0 pieces. We have verified his numerically by including n=2 components in rough accord with Fig.(3), and we find corrections less than 5%. The computer time savings due to neglect of these terms is of order 30%.

(D) Secondary Particle Production

Here we shall discuss the kinematics of the produced photons and neutrinos due to pion decay. This was previously discussed in ref.(20) (though we wich presently to correct a crucial typographical error in ref.(20); In eq.(14) of ref.(20) there is a subscript missing; the corrected form is:

$$dn_i/dE = \eta\,\theta(E_{\nu_i} - E)/E_{\nu_i} \tag{30}$$

The photons of π^0 decay in the CRLF have energies E_1 and E_2 such that $E_1+E_2=E_\pi$ and flat distributions in energy, corresponding to spherical decay distributions in the cm system. The photon energies are correlated, thus for a pair we have:

$$d^2N_\gamma/dE_1\,dE_2 = \int \delta(E_\pi-E_1-E_2)\,\theta(E_\pi-E_1)\theta(E_\pi-E_2) \cdot dN_{\pi^0}/dE_\pi\, f(E_\pi)\, dE_\pi \tag{31}$$

Integrating over E_π:

$$N_\gamma = 2N_{\pi^0} = \int dE_\pi (dN_{\pi^0}/dE_\pi) E_\pi f(E_\pi) \tag{32}$$

thus f(E) is determined and we have:

$$f(E_\pi) = 2/E_\pi \tag{33a}$$

$$dN_\gamma/dE_1 = \int \theta(E_\pi - E_1)\,\frac{2}{E_\pi}\,(dN_{\pi^0}/dE_\pi)\,dE_\pi \qquad (33b)$$

(this is a speedy way of deriving eq.(33); we refer the reader to ref.(22), noting our corrections to ref.(22) above, for more details) This is an essential result which we implement numerically to compute the produced photon distribution.

For the case of neutrinos from $\pi^\pm$ decay, we see that the process proceeds first through the decay $\pi \to \mu\nu$. The muon then undergoes the three body decay, $\mu \to e\nu\bar{\nu}$. Kinematically the muon in the CRLF has $E_\mu^+ \le E_\mu \le E_\mu^-$. and satisfies:

(34)

$$dN_\mu/dE_\mu = \frac{1}{2}\int \theta(E_\mu^+ - E_\mu)\,\theta(E_\mu - E_\mu^-)\,(E_\mu^+ - E_\mu^-)^{-1} \cdot (dN_\pi/dE_\pi)\,dE_\pi$$

Neglecting the mass of the electron the three body decay distribution satisfies:

$$dN_{\nu_e}/dE_1\,dE_2\,dE_3 = \int \delta(E_\mu - E_1 - E_2 - E_3)\,\theta(E_\mu - E_1)\,\theta(E_\mu - E_2) \cdot f'(E_\mu)\cdot\theta(E_\mu - E_3)\,dN_\mu/dE_\mu \cdot dE_\mu \quad (35)$$

Integrating eq.(35) we find the electron neutrino differential distribution in terms of the muon distribution. Since the muon mass is comparable to the pion, we may approximate the muon distribution by $dN_\mu/dE \approx dN_\pi/dE$, hence:

$$dN_{\nu_e}/dE \cong \int E_\pi^{-1}\, dN_\pi/dE_\pi\, dE_\pi \quad (36)$$

Hence, we see that the electron neutrino distribution is identical to the photon distribution to a factor of 2 in overall normalization. We will employ this approximation in our numerical analysis.

(E) Other Energy Loss Mechanisms

In addition to photomeson production we consider presently the energy loss due to (i) Compton scattering (ii) collisions with ambient nucleons (iii) collisions with starlight photons (iv) synchrotron energy loss in galactic and intergalactic B-fields (v) energy loss due to pair production (e^+e^- production) interactions (vi) effective energy loss due to redshift; we devote section IV to a general discussion of all cosmological effects. Only (v) will be seen to be significant. The

approximate criterion for a given energy loss mechanism to be relevant is $(E^{-1}dE/dx)^{-1} < R_H\gamma \sim 3\times10^{28}$cm. We will implement (v) and (vi) in our numerical evolution routine in a manner similar to the earlier treatments of photoproduction discussed in section II. This is valid here because the inelasticity and total cross-sections are slowly varying functions of energy.

(i) Compton scattering. The collision of a cosmic ray nucleon with $E > 10^{18}$ev and a 2.7^{o}K photon can lead to Compton scattering. This is a small effect relative to photoproduction, but has no high energy threshold. The inelasticity is so small that the process becomes negligible. Taking $\sigma_{Thompson} = 8\pi\alpha^2 m_p^{-2}/3 = 1.79\times10^{-31}cm^2$ and $\rho_\gamma = 400/cm^3$ we obtain the collision mean free path, $\ell = 1.4\times10^{28}$cm. However, the mean inelasticity is of order:

$$\eta = \tfrac{1}{2}(1 - E_p'/E_p) \sim E_{3^oK}E_p/(2E_{3^oK}E_p + m_p^2) \sim 2.7\times10^{-4} \qquad (37)$$

for $E_p \sim 10^{18}$ev. Thus, the relevant quantity, the energy attenuation length, becomes $(E^{-1}dE/dx)^{-1} \sim \ell\eta \sim 5.2\times10^{31}cm \gg R_H$.

(ii) Collisions with ambient gas. Taking a stationary nucleon as target, we may assume that the total cross-section for nucleon-nucleon scattering at 10^{10}Gev is bounded by $\sim$100mb. The cosmological limit on ambient nucleons is $\sim 10^{-6}/cm^3$, hence the mean free path is 10^{31}cm. At high energies we expect the incident nucleon to retain a large fraction of its energy, $\langle x_F \rangle \sim .9$, thus the inelasticity is $\sim .1$ and the energy attenuation length becomes 10^{32}cm. Encounters wih galaxies are

infrequent $\sim$ (galactic size/galactic spacing)^3 $\sim 10^{-6}$, while the density of baryons also rises by 10^6. However, even in galaxies we see that the energy attenuation length grossly exceeds the galactic size, hence the effect is negligible.

(iii) Collisions with starlight. The galactic energy density of starlight is comparable to that of the 2.7°K photons, and since the energy of starlight photons is 10^3 to 10^4 times the 2.7°K energies, the density is O(.4 to .04 cm^{-3}). Assuming the asymptotic photoproduction cross-section of 120 μb, and an inelasticity of $\sim$.1 we obtain $(E^{-1}dE/dx)^{-1} \sim 2\times10^{29}$cm. However the rarity of galactic encounters increases this cosmologically by another factor of 10^6.

(iv) Synchrotron energy loss. The Lienard result for power loss in an orbit of Larmor radius R is $P = 2e^2c\gamma^4\beta^4/3R^2$. The Larmor radius for a proton is 10^5cm(E Gev/B gauss) and we thus obtain in natural units:

$$(dE/dx)E^{-1} = \frac{8\pi}{3}\alpha(E\,(GeV))(B(gauss))^2\cdot(2\times10^{-24})\,cm$$

$$\simeq 1.22\times10^{-25}(E\,Gev)(B\,gauss)^2\ cm \qquad (38)$$

Typically, the cosmological B-field is assumed to be no greater than 10^{-9}gauss, which leads to an energy attenuation length of 10^{34}cm at 10^9Gev. In galaxies this becomes 10^{28}cm, but such encounters are rare ($\times10^{-6}$) and the attenuation length in the galaxy greatly exceeds its scale size, so trapping will not occur (of course, above 10^{15}ev leakage of nucleons is usually assumed).

(v) We include the important effect of electron positron pair creation. Here we rely heavily upon the analysis of Blumenthal[9] and the estimate of the mean energy attenuation length, (eq.(19) of ref.(6)). Our procedure is not to perform the average with the $2.7^{o}K$ distribution to obtain an average dE/dx, but rather to compute dE/dx for a given value of the longitudinal photon energy. For a bin size ΔE and photomeson interaction length dr, the number of particles leaving bin $(E,E+\Delta E)$ and recoiling into bin $(E-\Delta E,E)$ is then the fraction $(dE/dx(E))(dr/\Delta E)$. The energy binning and dr must be sufficiently small so that this fraction does not exceed $\sim.1$ in practice. We then perform the averaging over the photon energies in a loop external to both the pair production and photoproduction evolutions. This involves fitting Blumenthal's function, $\phi(\xi)$, which we do with an exponential over the range $.4 < \log\xi < 4.0$ (see Fig.(2) of ref.(9)). Here ξ may be regarded as the longitudinal energy of the photon.

(G) Numerical Analysis

Our numerical integration routine, COSEV, is a simple and straightorward application of the ideas discussed in this section. We bin the nucleon and pion energies, typically into 300 bins between the minimum produced pion energy, $z_{\pi}^{(-)}$, and a choice of upper limit, e.g. $3x10^{20}$ev. We have tested the insensitivity of our results to the binning size by running tests in bin numbers ranging from 100 to 1000. We bin the photon longitudinal energies into 10 to 20 bins ranging from .1 $T_{2.7^{o}K}$ to .4 $T_{2.7^{o}K}$. The slowest part of the numerical procedure is in

the evaluation of the integral on the rhs of eq.(9) for each energy bin. We have found that a cubic Simpson's rule integration routine works fine; converting to a log(E) variable is somewhat less stable numerically. Generally the effects of finite energy bin size become problematic below 100 bins, and 10 photon energy bins. Above 200 bins our precision is better than a few percent. The integration of transport equations of this kind with power-law distributions is a particularly benign problem numerically. Nonetheless, it is extremely difficult to get any useful analytical results.

We keep track of total nucleon number, interacting nucleon number and produced pion number. By separately counting the number of interacting nucleons and the number of produced pions, which should be equal, we essentally test the precision of the nested integrations such as described above. We also keep track of the total energy. With 300 bins these quantities are controlled to 5% precision over 100 interaction lengths.

IV. Cosmological Evolution

(A) Source Summation

We define the differential particle flux at redshift, z=0, for a source at distance R_o and "activity" $\eta = \eta(E_o)$=(the integrated number of produced particles with $E \geq E_o$ per second) to be:

$$j(E) = \frac{1}{4\pi R_o^2}\eta_o f(E); \qquad \int_{E_o}^{\infty} f(E)\,dE = 1 \tag{39}$$

The integrated flux is then:

$$I(E) = \frac{1}{4\pi R_o^2}\int_{E}^{\infty} f(\bar{E})\eta_o\, d\bar{E} \tag{40}$$

Generally we shall assume that f(E) has a cut-off E_c such that $f(E>E_c)=0$, and we shall write $f(E)=f(E_c,E)$.

The cut-off energy in the case of photoproduction and pair creation (relativistic photon targets) is determined by the photon temperature and we have $E_c \propto 1/T$. A source located at redshift z_o, cosmic coordinate r, observed at the present time, t_o, will produce a flux (we follow Weinberg[26], chapters 14 and 15):

$$j(E) = \frac{\eta(z)}{4\pi R(t_o)^2 r^2}\cdot f\left(E_c(1+z)^{-1}, E(1+z)\right) \tag{41}$$

where we've introduced a z-dependent activity:

$$\eta(z) = (1+z)^m \eta_0 \theta(\bar{z}-z); \quad \rho(z) = (1+z)^3 \rho_0 \qquad (42)$$

and the evolution of the source density $\rho(z)$ is also indicated.

The activity exponent, m, is characteristic of "bright phase models"[27,28,29], and we will find that the fits to the cosmic ray spectrum assuming the crosss-over energy is less than 10^{18}ev will require $m \geq 4$. The known activity of quasi-stellar objects to redshifts of order 2, where the activity is 100x greater than at $z \sim 0$ suggests that such an exponent is reasonable (see Schmidt in ref.(28)). Also, radio source counts suggest enhanced brightness of galaxies at smaller redshifts[26,29]. We also see that $\eta(z)$ involves a parameter, $\bar{z}$, which is the redshift of maximum activity. Our choice of the dependence upon this parameter is simply a guess since nothing is known about it. We will find, however, that the induced neutrino spectrum will exhibit an energy dependence that is sensitive to $\bar{z}$ and might ultimately allow a measurement of it. We note that Hillas[7] and Blumenthal[9] have previously considered values of $\bar{z}$ as great as $\sim$100.

The flux at the present epoch may be written as a volume integral in a Friedmann-Robertson-Walker metric (Weinberg[26], eq.(15.3.3) and below):

$$j(E) = \rho_0 \eta_0 c \int_0^{\infty} \frac{(1+z)^{m+3}}{4\pi R(t_0)^2 r^2} f\left(\frac{E_c}{(1+z)}, E(1+z)\right) \frac{4\pi R(t_e)^2 r^2 dr}{\sqrt{1-Kr^2}} \cdot \theta(\bar{z}-z) \qquad (43)$$

which upon using:

$$\frac{dt}{R(t)} = \frac{dr}{\sqrt{1-Kr^2}}\,; \quad \frac{dz}{dt} = -(1+z)^2\left(1+2q_0 z\right)^{1/2} H_0 \qquad (44)$$

becomes:

$$j(E) = \rho_0 \eta_0 c H_0^{-1} \int_0^{\bar{z}} \frac{(1+z)^{m-1}}{(1+2q_0 z)^{1/2}} f\left(E_c(1+z)^{-1}, E(1+z)\right) dz \qquad (45)$$

Eq.(45) reveals the interesting result that for $E_c(1+\bar{z})^2 \leq E \leq E_c$, the injection spectrum index, γ is modified to an observed index of $\gamma' = (m+\gamma-1/2)/2$. For in injection index of $\gamma = 2.0$ (2.5) we see that $\gamma' = 3.0$ implies that $m = 4.5$ (4.0). These are not unreasonable bright phase exponents[28,29].

It is useful to consider θ-function approximations to the spectrum where: $\theta(x>0)=1$; $\theta(x<0)=0$; $\partial\theta(x)/\partial x = \delta(x)$. Hence, we write:

$$f(E) \equiv f(E_c, E) = \alpha E^{-\gamma}\theta(E_c - E) \tag{46}$$

and eq.(45) becomes:

$$j(E) = [\rho_o \eta_o c H_o^{-1} \alpha E^{-\gamma}] \int_0^{\bar{z}} \frac{(1+z)^{m-1-\gamma}}{(1+2q_o z)^{1/2}} \theta(E_c - (1+z)E)\, dz \tag{47}$$

In flat cosmologies such as are predicted in inflationary scenarios we have $q_o = 1/2$. Assuming this greatly simplifies our analysis and eq.(47) becomes:

$$\hat{j}(E) = [\rho_o \eta_o c H_o^{-1} \alpha E^{-\gamma}] (m-\gamma-\tfrac{1}{2})^{-1} \left\{ \left[(1+\bar{z})^{m-\gamma-\frac{1}{2}} - 1 \right] \theta(\cdots \right.$$
$$\left. \cdots E_c - (1+\bar{z})^2 E) + \left[\left(\frac{E_c}{E}\right)^{\frac{m}{2}-\frac{\gamma}{2}-\frac{1}{4}} - 1 \right] \theta(E(1+\bar{z})^2 - E_c)\, \theta(E_c - E) \right\} \tag{48}$$

The utility of eq.(48) resides in the fact that any function may be written:

$$f(E_c, E) = \int_{E_o}^{\infty} g(E_c, \tilde{E})\, \theta(\tilde{E} - E)\, d\tilde{E} \qquad (49)$$

where:

$$g(E_c, E) = -(\partial / \partial E)\, f(E_c, E) \qquad (50)$$

and the observed spectrum becomes:

$$j(E) = \int_{E_o}^{\infty} g(E_c, E')\, \hat{j}(E', E)\, dE' \qquad (51)$$

hence $\hat{j}(E_c,E)$ is an effective Green's function for our problem. Introducing a generalization of eq.(46):

$$f(E_c, E) = \alpha E^{-\gamma} q(E_c, E) \qquad (52)$$

and assuming that the only scales present in $q(E_c,E)$ are E_c and E, that $q(E_c,E)$ has scaling dimension zero, i.e., $q(\lambda E', \lambda E) = q(E',E)$, we obtain for eq.(45) with $q_o=1/2$:

$$j(E) = \frac{1}{2}\rho_0 \eta_0 c H_0^{-1} \alpha E^{-\gamma-1} \int_E^{E(1+\bar{z})^2} \left(\frac{x}{E}\right)^{\frac{1}{2}(m-\frac{5}{2}-\gamma)} q_t(E_c, x)\, dx \qquad (53)$$

This is our basic result for this section which we use for the evaluation of the cosmological component of the spectrum.

Our heuristic argument for the pile-up in Section II indicates theat indeed the evolved nucleon spectrum will possess the scaling properties required for the validity of eq.(53). The heuristic argument indicates that q(E',E) will have the approximate form:

$$q_t(E_c, E) \cong \Theta(E_c - E) + \Theta\left(E - \left(1 - \frac{m_\pi}{m_p}\right)E_c\right) \cdot \Theta(E_c - E)\, m_p/(\gamma-1)m_\pi \qquad (54)$$

which satisfies the scaling requirement for q(E',E). Since we begin with a simple power law at injection and evolve q(E',E) and we conserve baryon number, we may normalize q(E',E) by:

$$\int_{E_0}^{\infty} q_t(E_c, E)\, E^{-\gamma_i} dE = (\gamma_i - 1)^{-1} E_0^{1-\gamma_i} \equiv \alpha^{-1} \qquad (55)$$

Eq.(53) defines a diffuse nucleon spectrum which we may fit to the observed differential spectrum for given values of z, m, and γ_i, to determine the quantity:

$$\Omega_{diffuse} = \rho_o \eta_o c H^{-1} \alpha \qquad (56)$$

We find generally, because of the "ankle" and the associated anisotropy, that the assumption of an exceptionally nearby or bright source is required, e.g. the Virgo supercluster, to obtain a complete fit. From eq.(39) with a fit including this component we obtain a result for:

$$\Omega_{local} = \eta_o \alpha (4\pi R_o^2)^{-1} \qquad (57)$$

Thus, knowing R_o and Ω_{local} we determine $\eta\alpha$. Knowing only Ω_{local} and $\Omega_{diffuse}$ we determine:

$$\omega \equiv \Omega_{diff}/\Omega_{loc} = 4\pi R_o^2 \rho_o c H_o^{-1} = 4\pi R_o^2 R_{IC}^{-3} c H_o^{-1} \qquad (58)$$

From this result and assuming that the cosmological sources are uniformly distributed throughout space with average separation interval at present of R_{IC}, using $\rho_o = 1/(R_{IC}^3)$, we deduce the ratio R_{IC}/R_o.

(B) The Normalization Problem

We have found the problem of the overall spectrum normalization to be sufficiently tricky that we devote the present disscussion to it. We also define here a number of functions which we compute numerically and which are related to the diffuse nucleon and neutrino differential and integral fluxes through normalization factors which contain the interesting source properties.

Consider a point source at a distance R_o. We have defined the observed differential flux for the source to be:

$$j(E) = \frac{\eta_o \alpha}{4\pi R_o^2} \left(\frac{E_0}{E}\right)^{\gamma_i} q_t(E_c, E) \equiv \Omega_{local} \left(\frac{E_0}{E}\right)^{\gamma_i} q_t(E_c, E) \tag{59}$$

in accord with the definition of $q(E_c,E)$ above. We shall take the reference energy E_o to be 10^{18}ev in practice.

We introduce the dimensionless function:

$$D(E) \equiv D(E_c, E) \equiv \frac{1}{2}\left(\frac{E_0^{\gamma_i}}{E^{\gamma_i+1}}\right) \int_E^{E(1+\bar{z})^2} \left(\frac{x}{E}\right)^{\frac{1}{2}(m-\gamma-\frac{5}{2})} q_t(E_c, x)\, dx \tag{60}$$

and the diffuse cosmological component is then:

$$j(E)_{diffuse} = \Omega_{diff} D(E) \tag{61}$$

Typically the data is plotted in the form $(E/E_o)^3 j(E)$. We fit this to the result:

$$\left[\frac{E}{E_o}\right]^3 j(E)_{observed} = \left[\frac{E_o}{E}\right]^{\gamma-3} q_t(E_c, E)\Omega_{local} + \left[\frac{E}{E_o}\right]^3 D(E)\,\Omega_{diffuse} \tag{62}$$

It is also convenient to consider the integrated flux I(E). for a typical differential spectrum of the form:

$$j(E) = \left[\frac{E_o}{E}\right]^{\gamma} \cdot \theta(E_c - E)\,\Omega_{local} \tag{63}$$

were $E_c >> E_o$ we have:

$$I_{local}(E_o) = \Omega_{local}\left(\frac{E_o}{\gamma-1}\right)\left(1-\left(\frac{E_o}{E_c}\right)^{\gamma-1}\right) \approx \Omega_{local}\left(\frac{E_o}{\gamma-1}\right) \tag{64}$$

Similarly, the diffuse spectrum may be written:

$$D = \int_{E_o}^{\infty} \frac{dE}{E_o} D(E) \quad ; \qquad I_{diffuse}(E_o) = \Omega_{diffuse} E_o D \tag{65}$$

The quantity D must be computed numerically after we fold in the redshift effects as in eq.(47). However, for the simple θ-function spectrum of eq.(46) we have:

$$D(E) = (m-\gamma-1)^{-1}\left\{\left[(1+\bar{z})^{m-\gamma-\frac{1}{2}}-1\right]\theta(E_c-E(1+\bar{z})^2) + \left[\left(\frac{E_c}{E}\right)^{\frac{m}{2}-\frac{\gamma}{2}-\frac{1}{4}}-1\right]\theta(E(1+\bar{z})^2-E_c)\,\theta(E_c-E)\right\} \tag{66}$$

and, assuming $E_o(1+\bar{z})^2 > E_c$ (or $\bar{z} > 9$) we find:

$$D = \left[(p-1)^{-1}\left(\frac{E_c}{E}\right)^{p} - p(p-1)^{-1}\left(\frac{E_c}{E}\right) + 1\right](2p)^{-1} \quad (67)$$

where $p=m/2-\gamma/2-1/4$ and typically $\gamma=2.5$, $m=4.0$ so $p=1/2$. Therefore:

$$I(E_o)_{observed} = \Omega_{local}\frac{E_o}{\gamma-1}\left(1-\left(\frac{E_o}{E}\right)^{\gamma-1}\right)$$

$$+ \Omega_{diffuse}(2p)^{-1}\left[\left(\frac{E_c}{E}\right)^{p}(p-1)^{-1} - p(p-1)^{-1}\left(\frac{E_c}{E}\right) + 1\right] \quad (68)$$

(here γ is the injection slope, not the observed slope).

In general we will distinguish between the cut-off in the local component and the cut-off in the diffuse component. This is due to the fact that the effects of pair-creation have little impact upon the local contribution, but will significantly reduce the cut-off in the diffuse component.

For the ν_e spectrum we first note that we can directly compute the ratio of induced ν_e's to nucleons at range R_o:

$$I_{\nu_e}(E\geq 0)/I_N(E_o) = c(\gamma_i, E_o)f(R_o) \quad (69)$$

by numerical integration of the spectrum evolution transport equations. Here $f(R_o)$ is the fractional yield of neutrinos produced at range R_o and $f(\infty)=1$. We derive $c(\gamma_i,E)$ and f numerically and give results in Table I. We define the ν_e spectrum induced from a point source of nucleons at range R_o to be:

$$j_{\nu_e}(E) = \frac{\eta_o \varepsilon f(R_o)}{4\pi R_o^2} S(E_c, E) = \Omega_{local} f \varepsilon S(E_c, E) \tag{70}$$

where $S(E_c, E)$ is the function of Fig.(8b) with the normalization $S(E_o, E_o)=1.0$. This function is weakly dependent upon the injection index of the nucleon spectrum, unless one is interested in the highest energy neutrinos, $>10^{19}$ev. The properties of this function are derived numerically in the next section, but we note that fig.(9) displays the departure from universality of the high energy end of the neutrino spectrum for different injection indices.

The integrated ν_e flux is then:

$$\int_0^\infty j_{\nu_e}(E)\, dE = \Omega_{local} f \varepsilon T(E_c); \quad T(E_c) \equiv \int_0^\infty S(E_c, E)\, dE$$

$$T(E_c) \equiv E_o T \tag{71}$$

and the numerical result for the normalization constant, T, is found to be T=10.67. Hence:

$$I_{\nu_e}(0)_{loc}/I_N(E_o)_{loc} = f\varepsilon(\gamma-1)T = fc(\gamma_i, E_o)$$

$$\varepsilon = c(\gamma_i, E_o)/(\gamma-1)T \qquad (72)$$

Thus the local differential spectrum is:

$$j_{\nu_e}(E) = \Omega_{local}\left[c(\gamma_i, E_o)/(\gamma-1)T\right] S(E_c, E) f(R_o) \qquad (73)$$

The diffuse cosmological ν_e spectrum may be obtained with the aid of eq.(53). Note first that $\gamma=0$. Second, the differential ν_e spectrum produced at redshift 1+z, observed at z=0 will take the form:

$$j_{\nu_e}(E, z) = \frac{\eta(z)}{4\pi R^2(0) r^2} (1+z)^{\gamma+1} S(E_c, E(1+z)^2)\,\varepsilon \qquad (74)$$

$$(f \approx f(\infty) = 1)$$

This is due to the fact that it is $I_{\nu_e}(0)/I_N(E_o/(1+z))$ that remains constant and thus the produced ν_e's will be in a greater abundance by a factor of $(1+z)^{\gamma-1}$ at redshift z, following the increased integrated number of active nucleons as the threshold is reduced. But, the reduction in threshold gives an effective reduction in T by a factor of $1/(1+z)^2$ (we integrate in eq.(71) up to an upper limit of $E_c/(1+z)^2$; this is the effective increase in the normalization of the function $S(E_c,E)$ as E_c is reduced to $E_c/(1+z)^2$).

Again, it is useful to introduce a dimensionless function, $G(E_c, E)=G(E)$ by:

$$G(E) = \frac{1}{2}\int_{E}^{E(1+\bar{z})^2} \left(\frac{x}{E}\right)^{\frac{1}{2}(m-\frac{3}{2}+\gamma_i)} S(E_c, x)\,\frac{dx}{E} \qquad (75)$$

and the normalization constant is defined:

$$G \equiv \int_{E_o}^{\infty} G(E_c, E')\,\frac{dE'}{E_o} \qquad (76)$$

Therefore, the cosmologically evolved neutrino differential spectrum becomes:

$$j_{\nu_e}(E)_{diffuse} = \left[c(\gamma_i, E_o)/(\gamma_i-1)T\right]\Omega_{diffuse}\,G(E) \qquad (77)$$

where $\gamma_i = \gamma_{injection}$.

Remarkably we see in eq.(75) that the bright phase parameter m and the injection nucleon index γ_i enter in the combination $m+\gamma_i$. This is related directly to the observed cosmic ray spectrum slope by $\gamma_{observed}=(m+\gamma_i-1/2)/2$. Hence, the neutrino spectrum only depends upon the observed nucleon index, and we see in eq.(75) that to a very good approximation the slope of the produced diffuse neutrino spectrum will be $\gamma_o+(1/2)$. We may write for the integrated diffuse ν_e component

above the reference energy E_o:

$$I_{\nu_e}(E_o) = E_o G \varepsilon \Omega_{diffuse} = \left[\frac{c(\gamma_i, E_o) G}{2(\gamma_i - 1) T D}\right] I_{N\,diff}(E_o) \tag{78}$$

The parameters defined presently are numerically evaluated in the following section. The forms derived by θ-function approximations are generally sufficiently accurate for analytic estimates.

V. Numerical Results

In figures (4) through (6) we present the results of evolving injection spectra with indices γ_i =3.0 through 2.0 using the full transport evolution equations while neglecting cosmological effects. 1 il. (interaction length) corresponds roughly to 6 Mpc and 500 il. roughly corresponds to R_H, the Hubble length scale. Thus, the neglect in redshift effects in these figures makes them inapplicable as final results beyond 100 Mpc or about 12 to 24 il. However, these are suitable results for nearby sources and as inputs to the formulae of section IV for the computation of redshift effects. All of these results were obtained with the spherically symmetric angular distribution assumption for photomeson production, and with Blumenthal's results for pair creation[9].

Figure (4) contains an evolved $1/E^{3.0}$ injection spectrum. To a good approximation this is equivalent to the result for $q(E_c,E)$ for injection spectra with slopes as flat as 2.0. We assumes an artificial

numerical cut-off of $3x10^{20}$ev (at most a 10% normalization correction above 10^{20}ev). After 3 il. the appearance of the cut-off and the pile-up are easily seen. The pile-up peak reaches a maximum at a range of order 24 il. Here it is about 1.6x the flat injection spectrum lying in the range 3.0 to 5.0 $x10^{19}$ev. Beyond this range the effects of pair creation become pronounced. We see the gradual shifting of the pile-up toward lower energies and the remarkable new feature: the appearance of a "dip" onsets at .7 to 2.0 $x10^{19}$ev. The dip occurs because here we see the peaking of the pair-creation energy loss effect (see Blumenthal, ref.(9) fig.(4)) while the large "pile-up" remains above this energy scale. The result is much like that of a snake digesting a small pig, and the pile-up slowly moves to lower energies while the spectrum is significantly reduced at slightly lower energies. The pile-up is not easily "digested" and remains quite conspicuous out to even 500 il. By 144 il the pile-up drops below the normalization of the input spectrum.

In figure (5a) we present the evolution of the $1/E^{2.5}$ injection spectrum. The function $q(E_c,E)$ can be inferred by subtracting the injection spectrum from the plotted spectrum in the log plot. In Fig.(5b) we present the high energy end of the spectrum and show our artificial numerical cut-off on the injection spectrum. Unfortunately, we become increasingly sensitive to this cut-off as the injection slope is reduced, and we have not carried out runs with a numerical cut-off much larger than $3x10^{20}$ev. Thus, our results above 10^{20}ev should not be taken too seriously, and for $1/E^2$ injection slope they are expected to have 30% corrections.

In fig.(6) we present the $1/E^{2.0}$ injection slope results, and our ordinate scale is changed to accomodate the results. Thus, the dip and pile-up are less conspicuous here but do occur with approximately universal structure after 100 il. We have not run $1/E^{1.5}$ injection spectra, or flatter, but may infer the general behavior of such from the $1/E^{2.0}$ results. We realised after the completion of our figures that we should probably be presenting the data in terms of the scale invariant function, $q(E_c,E)$ defined in section IV, but one can extract this function from the presented data in the figures.

In fig.(7) we present the evolution of the number of produced secondary electron neutrinos with range for each of the injection spectra. The injection spectra are each normalized to unity at 10^{18}ev thus the asymptotic values plotted in fig.(7) represent the quantity $c(\gamma_i, 10^{18}\text{ev})$ defined in section IV. Obviously the neutrino yield increases with the flattening of the injection spectrum and closely follows the integrated number of nucleons above 10^{20}ev in the injection spectrum, i.e. we see that the neutrino yields are in the ratio 1:10:100 for injection indices 3.0:2.5:2.0. We have previously run simulations without the effects of pair-creation and found that many more secondary neutrinos were produced and that the approach to asymptopia is much slower. The pair creation effects, by reducing the pile-up to lower energies, accelerates this approach, and thus simplifies our problem of including the red-shift and cosmological source sums.

In fig.(8a) we present the successive pile-up of produced pions with an arbitrary normalization (which we do not require, but which must be consistent with the normalizations of Fig.(7) for the integrated

spectra). In fig.(8b) we give the neutrino spectrum with range, or equivalently the function $S(E_c,E)$ defined in section IV, which is normalized to unity at E=0. The resulting $S(E_c,E)$ is essentially independent of the injection slope for energies less than 10^{19}ev.

However, there are departures from universality for various injection spectra in $S(E_c,E)$ above 10^{19}ev as is seen in fig.(9). Obviously, the flatter injection spectra produce a more copious yield of UHE neutrinos. However, if one measures the slope of $S(E_c,E)$ above 10^{19}ev one finds a rapid cut-off of $\sim 1/E^{4.0}$. This is essentially the effect of the kinematics of the produced pion as seen in fig.(1) and in the produced pion distributions of fig.(8a), and thus the search for electron neutrinos above 10^{19}ev produced by this mechanism would not be too promising. Since it is difficult to imagine any other mechanism for producing UHE neutrinos (they are uncharged and do not participate in dynamo effects; other collision processes are unlikely as per section III.) the interesting range to study would appear to be 10^{18}ev up to 10^{19}ev.

Since a universal differential neutrino spectrum is produced after a few tens of interaction lengths by any given source with a normalization that is simply related to the injection slope, it becomes a simple matter to compute the cosmological neutrino flux of unit normalization, i.e. we present the function $G(E_c,E) = G(E)$ in fig.(10) as defined in section IV. In using this result to predict an observable neutrino flux, we first determine the coefficient of the cosmological nucleon flux component, Ω_{diff}, and write:

$$j_{\nu_e\,diff}(E) = \Omega_{diff}\left(\frac{c(\gamma_i,E_o)}{(\gamma_i-1)T}\right)G(E) = I_{N\,diff}(E_o)\left(\frac{c(\gamma_i,E_o)}{(\gamma_i-1)TDE_o}\right) \cdot G(E) \qquad (79)$$

for injection index γ_i. The quantity $c(\gamma_i,10^{18}ev)$ is tabulated in Table (I) for various injection indices and T=10.67 is the normalization of $S(E_c,E)$ divided by 10^{18}ev. D is the normalization of the diffuse component spectrum, D(E) and is also given in Table (I). Thus, for example, if the observed integrated spectrum above 10^{18}ev is $I_N(10^{18}ev)=I_{diff}(10^{18}ev)=I_o$, and if we take an injection index $\gamma_i=2.5$, then we find that $c(2.5,10^{18}ev)=2.17x10^{-3}$, and $D(2.5)=1.20$,we obtain:

$$j_{\nu_e}(E) = I_N(10^{18}ev)\,(10^{18}ev)^{-1}\,G(E)\cdot(1.103\times10^{-5}) \qquad (80)$$

As described in section IV, to a good approximation G(E) falls like $1/E^{3.5}$ above the energy scale $5x10^{18}ev/(1+\bar{z})^2$. Below this scale the spectrum must flatten, and its observation can in principle reveal the quantity $\bar{z}$. The actual high energy behavior of G(E) is presented in fig.(10b) and we readily see that above $2x10^{19}$ev the spectrum steepens and drops much faster than $1/E^{3.5}$. Our numerical evaluation is insensitive above this scale.

The integrated neutrino spectrum is given by:

$$I_{\nu_e}(10^{18}\,ev) = \frac{c(\gamma_i, 10^{18}_{ev})\, G}{(\gamma_i - 1)\, T\, D}\, \Omega_{diff}\, I_N(10^{18}_{ev}) \qquad (81)$$

and we thus obtain for the example above $I_{\nu_e}(10^{18}ev)=1.06x10^{-1}I_o$. The integrated flux falls roughly as $1/E^{2.5}$. In section VI. we will be fitting the nucleon spectrum with diffuse and local components and will obtain in this manner the induced neutrino spectra as corollary predictions.

In computing the cosmologically evolved nucleon spectrum we encounter an ambiguity. Our assumption in section IV was that the nucleon spectrum would undergo a rapid evolution due to photomeson production and then become stable. In that case, we would insert the stable fully evolved spectrum, $q(E_c,E)$, into eq.(60) for the function D(E) and obtain an unambiguous prediction for the diffuse spectrum. However, as figs.(4) through (6) reveal the spectrum is far from stable after 20 il. due to the effects of pair creation and the gradual shift of the pile-up to lower energies. Thus the dilemma arises in the present approximation (a more careful analysis should someday be performed which parameterizes this subsequent evolution) which spectrum at what range should be used as the input to eq.(60)?

A sum over distant sources either weights the nearest or the most distant sources preferentially. In the present case of a bright phase index m=4 to 5 we preferentially weight the most distant sources. Therefore, we might use the 500 il. spectrum as input since the 24 il spectrum would lead to an overestimate of the effective cut-off energy.

However, by doing this we somewhat underestimate the spectrum above $2x10^{19}$ev. This has the effect of overemphasizing the dip structure seen in the data. We've opted instead to use the approximate geometric mean of the two extremes, 144 il. as our input for $q(E_c,E)$. We've found that this does not qualitatively change the results, though the dip is least conspicuous with the 24 il. input. A better computation would input a "moving" q(E) with z, but then sacrifice the simplicity of eq.(60).

In fig.(11) therefore we present the result of the cosmological convolution integral, i.e. the function D(E) defined in section IV for the various injection spectra γ_i. Actually, we've made an additional approximation here which is to use the 144 il. function $q(E_c,E)$ derived from the $\gamma_i=2.0$ case for each injection spectrum. In actuality the cut-off should not be so abrupt at $2x10^{19}$ev, and it should not be exactly the same for each injection spectrum. However, these departures from universality should not be much more severe than those seen in the preceding examples. We find in section VI. that the $1/E^{2.0}$ fit is the best.

The normalization of the D(E) is given as the quantity D for energies above 10^{18}ev and clearly differs among the spectra.

V. A Model of the Ultra High Energy Spectrum

Armed with the analyses of Sections IV and V we are ready to attempt a model fit to the ultra high energy nucleon spectrum and to make predictions for the neutrino spectrum. Unfortunately we will be limited by the available data, but our approach is sufficiently general that it may be updated as more data accrues.

Throughout we will fit exclusively to the Haverah Park data as presented in Cunningham et.al.[16a] and Brooke et. al.[16b]. This is a matter of convenience; the Haverah Park data is the largest single and thus internally consistent set and we need not worry about relative calibration errors between different facilities. Nonetheless, we do not do justice to the existing data presently because we have not developed a detailed understanding of the experimental errors. We have inferred the error from a careful scrutiny of the figures in the principal references and comparisons of reported χ^2 estimates against our own. We feel a more complete error analysis would be of considerable use. Also, it is difficult to interpret the statistical variables when the errors are increasing monotonically with the energy; a χ^2 measurement above 10^{18}ev is virtually insensitive to the "ankle", while the relative normalizations of energy bins in the ankle are statistically significant.

Our idea presently is not new but our methods based upon the earlier discussions in this paper are. Thus our results are entirely new and supercede most previous analyses involving the GZ cut-off and induced neutrinos. We shall assume that the UHE cosmic ray spectrum is of a cosmological origin and composed of two components: (1) A diffuse cosmological component of strength $\Omega_{diff}D(E)$ which has been steepened

from an injection index γ_i to an observed γ_{obs}=3.0 bu the cosmological red-shift effects and the bright-phase activity discussed in section IV. This is the idea of Hillas[7] and implemented with pair production by Blumenthal[9] (2) A semi-local component which we write as Ω_{Virgo} x $q(E)/E^{\gamma_i}$, which we identify with the Virgo cluster as containing a source or sources at a range 3 il. wrt. photomeson production. This idea has been explored previously by Wolfendale and collaborators in ref.(8). One might go further to postulate a local component primarily composed of (Fe) originating within our galaxy and subject to the effects of local steering. Our assumption presently will be that the cross-over energy occurs at a scale small relative to 10^{18}ev and that only the cosmological and semi-local components appear at this energy. This is, of course, related to the redshift of maximum activity and for $E_{cross-over} < 10^{18}$ev we require $\bar{z} > 10$.

Why should we superimpose the diffuse component and the semilocal component? We find in our fits that the normalization of the diffuse component will imply an average source separation of order 100 Mpc. This is, remarkably, the scale of supercluster heirarchies. Of course, the Virgo cluster is only 20 Mpc in range and should be $\sim$25 times brighter than the first diffuse components. The diffuse component will cut-off at a scale of order $4x10^{19}$ev since it will be dominated by the effects of the most distant sources (there will be a correction of order 20% to this by our neglect of the nearest sources in the source sum integral, i.e. the nearer diffuse components don't cut-off until about $6x10^{19}$ev), while the semi-local component will be enhanced at $8x10^{19}$ev by the pile-up and the flatter injection index. Both the diffuse and semi-local components will produce neutrinos, and an anisotropy will

occur in the highest energies associated with the direction of Virgo.

It is conceiveable that the cross-over is just occuring at a scale of $\sim 10^{19}$ev in which case a three component model is required. Here we assume that the Virgo cluster is responsible for the anisotropy and is emerging as the ankle structure in the spectrum as well. But, we may then turn the argument around and assume a supercluster interspacing of order 100 Mpc for clusters of similar activity to Virgo to obtain an estimate of Ω_{diff}, and then to obtain a prediction for the neutrino spectrum, even though the diffuse contribution to the nucleon spectrum is masked by a local component. The result of this exercise will be similar to the results obtained here.

In fig.(12) we present the Haverah Park data, excluding the most recent events reported at the 18th ICRC[16]. To this data we fit the composite spectrum:

$$j_N(E) = \Omega_{diff} D_{\gamma_i}(E) + \Omega_{Virgo}\, j_{local}(E) \qquad (82)$$

where D(E) is the evolved diffuse spectrum function of fig.(11) and $j_{loc}(E)$ is the 3 il. evolved injection spectrum normalized to unity in fig.(4) through fig.(6). For tests with spectra flatter than 2.0 we assume the $q(E_c,E)$ obtained for the γ_i=2.0 case.

In fig.(12) we also show the results of our three best fits to this data. These correspond to γ_i=2.2, γ_i=2.0 and γ_i=1.8 respectively yielding χ^2= 2.94, 2.14 and 2.67. The best fit with γ_i=3.0 has χ^2=2.95 and results in Ω_{diff}=0.0. The χ^2 reported here is for all

bins above 10^{18}ev, while for those bins above $5x10^{18}$ev we obtain χ^2= (2.72,1.90,1.69) respectively. In Table(II) we present the results for the parameters of these fits.

In addition to the ankle, a striking result here is the appearance of the "dip" structure at the scale $\sim 10^{19}$ev. This structure is visually present and appears to be statistically significant. One can find the best straight line fit to the data above 10^{18}ev which has a χ^2 of 3.54, and corresonds to an ordinate of 1.06 in fig.(12). Above $5x10^{18}$ev the same straight line fit has a χ^2 of 3.07, while the best line now has χ^2=2.38 and an ordinate value of .95. With the existing statistics, these measures are not very meaningful and we await the accrual of more data.

The dip must always arise in our model because of the "mini-crossover" from the diffuse component to the semi-local one at about 10^{19}ev. However, as we mentioned in section IV., the ambiguity in the choice of an input $q(E_c,E)$ in the evaluation of D(E) slightly exaggerates the dip. We believe that the dip may ultimately be a reliable feature in the spectrum compelling this kind of a model. We note that in the spectrum figure of Cunningham et. al.[16a] the dip is visually present in all other data sets of other groups, and we encourage experimentalists to give it an unbiased study. We warn the reader that the dip (or even the ankle) may be a phenomenon associated with a rapid phase change in the anisotropy and the detector response to such. Thus, further experimental analysis of the hypothetical dip structure is needed.

We see that our fits give an ankle structure in qualitative agreement with the reported data, though statistically this result is not yet very meaningful.

We obtain directly from our fits the ratio:

$$\omega = \Omega_{diff} / \Omega_{local} = 4\pi R_V^2 \rho_o c H_o^{-1} \qquad (83)$$

where R_{Virgo} is the range of Virgo, 20 Mpc, and the Hubble length is $cH_o^{-1} = h_o^{-1}(3\times10^{\cdot})$Mpc, and ρ_o is the supercluster density $= 1/R^3_{IC}$ where R_{IC} is the interclusteral spacing. We find therefore:

$$R_{IC} = h_o^{-1/3}\,\omega^{-1/3}\cdot(2.47\times10^2\ Mpc) \qquad (84)$$

The natural expectation the $R_{IC}\sim$ 100Mpc emerges from our fits. Also, we have from the integrated normalizations of $j_{\gamma_i}(E)$ and the D(E) the result for the integrated flux above 10^{18}ev:

$$I_N(10^{18}_{ev})/10^{18}_{ev} = (\gamma_i - 1)^{-1}\Omega_{Virgo} + D_{\gamma_i}\Omega_{diff} \qquad (85)$$

$$= \Omega_{Virgo}((\gamma_i - 1)^{-1} + D\omega)$$

where D is given in Table(I). These parameters are given in Table(II).

From these results we obtain crude anisotropy estimates. In fig.(13) we plot:

$$a \equiv \frac{\Omega_{Virgo}\, j_{\gamma_i}(E)}{\Omega_{diff}\, D(E) + \Omega_{Virgo}\, j_{\gamma_i}(E)} \qquad (86)$$

for our three best fits. This assumes that pure Virgo cluster yields an anisotropy of 100% and pure diffuse yields 0% (a residual galactic contribution might show up here at low energies). We plot also the anisotropy data of ref.(16). Remarkably, our best spectrum fit appears to be in best agreement with the anisotropy as well, though we have not carried out a statistical comparison. It is interesting that the χ^2 minimum is closest to the reported anisotropy.

From the values of the parameters derived by the best fit to the spectrum, we can obtain predictions for the resulting electron neutrino spectrum and anisotropy. We have:

$$j_{\nu_e}(E) = \Omega_{Virgo}\,\varepsilon\,S(E) + \Omega_{diff}\,\varepsilon\,G(E) \qquad (85)$$

and the anisotropy:

$$a_{\nu_e} = \frac{\Omega_{Virgo}\cdot S(E)}{\Omega_{diff}\cdot G(E) + \Omega_{Virgo}\cdot S(E)} \qquad (86)$$

These are plotted in fig.(14).

The integrated flux of neutrinos above 10^{18}ev is then:

$$I_{\nu_e}(10^{18}\,ev) = (10^{18}\,ev)\,\Omega_{Virgo}\left[\,C(\gamma_i,E_0) + \omega G\varepsilon\,\right] \qquad (87)$$

where the parameters are given in Table(I).

The best fit to the spectrum with γ_i=3.0 excludes the diffuse component altogether. Nonetheless, for injection spectra nearly this steep we can argue that a diffuse component must exist with a density corresponding to $\sim$100Mpc interspacing of sources. This implies a lower limit on our neurtrino flux above 10^{18}ev of 1.0/km yr sr. This is pessimistically low. We obtained this result previously in ref.(22), though we overestimated the detectability therein.

Our best two-component spectrum fit predicts $I_{\nu_e}(10^{18})=.652I_N(10^{18}) \sim 1.65\times10^{-16}$ $cm^{-2}s^{-1}sr^{-1}$ and this may be assumed to fall like $1/E^{2.5}$ up to 10^{19}ev. Hence, $I_{\nu_e}(10^{19}\text{ev})=5.22\times10^{-18}cm^{-2}s^{-1}sr^{-1}$, a result within two orders of magnitude of the Fly's eye current upper limit for events above 10^{19}ev of $3.9\times10^{-16}cm^{-2}s^{-1}sr^{-1}$. Of course, better would be a comparable limit for events above 10^{18}ev where our spectrum is more active by 300x. Such a limit may be possible with an improved analysis of the LPM effect in earth and a recalculation of the total neutrino cross-section[30]. The extremely exciting possibility of observing the $I_{\nu_e}(10^{19})$ result consistent with a $1/E^{2.0}$ injection spectrum is clear. It would constitute very strong evidence for the picture described here. Also, the eventual mapping of the spectrum down to lower energies where it should eventually roll over to a flat form at $\sim 5\times10^{18}\text{ev}/(1+\bar{z})^2$, would constitute a measurement of $\bar{z}$. Though we have not presently discussed it, departures of the neutrino slope from 3.5 in the present model contain information about the ubiquitous deceleration parameter, q_o. In a future paper we will explore the cosmological possibilities further[31].

Thus we see that a cosmological window may be opening here. We have assumed $q_o=1/2$ throughout, but a more general analysis is possible. We assume $\bar{z}$ large in our discussion. The quantities h_o and m are also observables. With several orders of magnitude improvement in the data of this kind, such a model, if it survives, can in principle address the measurements of these quantities. No other astronomy would seem to focus upon exclusively the window $z \longrightarrow 10$ to 100.

VI. Results and Conclusions

We have provided a detailed analysis of the spectral evolution upon passage through the 2.7^{o} microwave background and the effects of the cosmological Hubble expansion on the spectrum and corollary phenomena. Let us summarize our principal conclusions.

(i) There is probably a cross-over energy $10^{15}ev < E_c < 10^{17 \text{ to } 19}ev$ at which the local galactic component of the spectrum, with relatively large (Fe) abundance, is exceeded by a cosmological diffuse component consisting mostly of nucleons.

(ii) The dominant effects in the long-range propagation and production of cosmic ray nucleons are (a) photomeson production (b) e^+e^- pair production and (c) redshifting of energy and bright phase production.

(iii) These effects should be treated in a transport formalism. Otherwise, important consequences such as the pile-up and dip will generally not appear. An injection spectrum with index γ_i will be steepened by the cumulative cosmological effects to an observed index of $\gamma_i/2 + m/2 - 1/4$ for bright phase parameter m. A pile-up of nucleons at about 4 to $7 \times 10^{19}ev$ will occur followed by the conventional GZ cut-off. The pile-up shifts to lower energies due to the effects of pair production after 24 il. A large dip appears at $10^{19}ev$ due to combined effects of pile-up and pair production.

(iv) The Haverah Park data has a statistically significant dip structure as well as the "ankle". These are fit well by two component models consisting of diffuse and semi-local parts, the latter when identified with the Virgo cluster gives excellent agreement with the reported anisotropy. We find that the $1/E^{2.0}$ injection spectrum gives

the best statistical fit to the data. The result $R_{IC} \sim 100$Mpc emerges from our fit to the data.

(v) A potentially detectable electron neutrino spectrum is predicted with a high energy anisotropy slightly less well pronounced than the UHE nucleon anisotropy. Limits on the integrated neutrino flux above 10^{18}ev may soon rule out injection indices smaller than 1.5. The neutrino spectrum has a universal slope of 3.5 up to 2×10^{19}ev, and a flattening below $5\times10^{18}\text{ev}/(1+\bar{z})^2$, and thus contains interesting information about the pre-Quasar epoch, i.e. the "bright phase maximum".

(vi) Most of our results are sufficiently general that they transcend the conclusions based upon the model fit. These methods will remain applicable to analyses of the spectrum as better and more data accrue.

The establishment of the UHE cosmic rays as a window on the early universe would be a great achievement, and should provide a strong impetus for further study with large facilities. Also, the possible discovery of certain exotica of a fundamental particle nature remains a possibility, though plays no role in our present analysis (see, eg. ref.(32) for a possible source of a diffuse injection spectrum of index 1.5, but with a much different corollary neutrino spectrum than described here; only such objects would seem to furnish sufficiently UHE neutrinos to implement Weiler's interesting idea of seeing the 2°K background neutrinos[33] however, our main conclusion presently is that few neutrinos are expected above 10^{19}ev which makes the prospect of detecting the neutrino background by this mechanism rather dim). UHE cosmic ray physics is currently underfunded and is nowhere near the

point of diminishing returns; the payback of further investment here stands to be quite significant.

Acknowledgements

We wish to thank the following people for useful information, discussions and encouragement throughout this lengthy project, about general aspects of CR physics as well as points specific to this work: Prof. J. Arafune, J.D. Bjorken, G. Cassiday, D. Cline, T. Gaisser, J. Linsley, J. Lloyd-Evans, E. Loh, C. Quigg, J. Rosner, P. Sokolsky, T. Stanev, A. Watson and G. Yodh.

FIGURE CAPTIONS

Fig.(1) Nucleon and pion kinematic regions for y=1 in terms of scaling variables as obtained in eq.(22) and eq.(23) of text. For calibration, if $T=2.7^{o}K$, then z=.1 corresponds to 3.35×10^{20}ev and the threshold, x=.081 corresponds to 2.7×10^{20}ev. However, $\langle y\rangle=3.2$, and the mean threshold is 8.47×10^{19}ev, which roughly corresponds to the cut-off obtained by numerical integration.

Fig.(2) Total photoproduction cross-sections in microbarns vs. laboratory photon energy, and x_N for $y=3.2$. (A) $\sigma_{total}(\gamma p\rightarrow all)$ (B) $\sigma(\gamma n\rightarrow \pi^- p)$ (C) $\sigma(\gamma p\rightarrow \pi^+ n)$ (D) $\sigma(\gamma p\rightarrow p\pi\pi)$ (E) upper limit to all final states with ≥ 3 pions on proton target. $\sigma_{total}(\gamma n)$ is inferred from $\sigma(\gamma D)$ (not shown) and is to a good approximation identical to $\sigma_{total}(\gamma p)$.

Fig.(3) Coefficients a_0, a_1, a_2 in expansion of $d\sigma/d\Omega$ for $\gamma p\rightarrow \pi^o p$ (eq.(26)) in μb/ster vs. E_{lab} taken from Genzel and Pfeil[25]. Also shown (dotted) are our fits for the spherically symmetric approximation and the test cases keeping both a_0 and a_2.

Fig.(4) Evolved $1/E^{3.0}$ injection spectrum to 500 interaction lengths. 1 il.= 6Mpc; Log to base e in ordinate. Injection spectrum is normalized to unity at 10^{18}ev. This may be taken as a good approximation to $q(E_c,E)$ for $\gamma_i = 2.0$

Fig.(5a) Evolved $1/E^{2.5}$ injection spectrum normalized to unity at

10^{18}ev. 1 il.= 6Mpc; Log to base e in ordinate. The dip structure and the downward evolution of the pile-up with increasing range are clearly seen.

Fig.(5b) High energy behavior of $1/E^{2.5}$ injection spectrum. Note that injection spectrum is cut-off at $3x10^{20}$ev.

Fig.(6) Evolved $1/E^{2.0}$ injection spectrum normalized to unity at 10^{18}ev. 1 il.= 6Mpc; Log to base e in ordinate.

Fig.(7) Neutrino yield with range for (A) $1/E^{2.0}$ (B) $1/E^{2.5}$ (C) $1/E^{3.0}$ injection spectra. This is the function $2\{c(\gamma_i, E_o)=I_{\nu_e}(0)/I_N(10^{18})\}$. The numbers refer to the asymptotic yields used in normalizing the cosmological neutrino spectrum. The approach to asymptopia is slower without the pair-production effects and higher neutrino yields would occur.

Fig.(8a) The evolution of the differential pion distribution from which we derive the differential neutrino (and photon) distributions. We establish the normalizations of these latter distributions separately, and the pion distributions here have arbitrary normalization.

Fig.(8b) Evolution of the neutrino differential spectrum with range normalized to unity at $E \rightarrow 0$. This is the function $S(E_c,E)$ defined in Section IV used in computing the cosmological flux. This plot is for the case of a $1/E^{2.5}$ injection spectrum, but the result is universal below 10^{19}ev.

Fig.(9) Departure from universality in $S(E_c,E)$ at high energy is seen here for different input spectra. Since fluxes are so low at these energies, we neglect these effects.

Fig.(10a) The cosmological neutrino spectrum with "unit normalization", i.e. this is the function $G(E_c,E)$ defined in Section IV, evaluated for different maximum brightness redshifts, z. The curves become universal at high energies. In principle, the observation of the roll-over would constitute a measurement of $\bar{z}$. $q_o=1/2$ is assumed. The high energy slope is $\gamma_{observed}+(1/2)$, independent of m and $\gamma_{injection}$.

Fig.(10b) High energy behavior of $G(E_c,E)$ and $S(E_c,E)$ for comparison. We assume a universal $S(E_c,E)$ for the evaluation (we use $\gamma_i=2.5$ as in Fig.(9)).

Fig.(11) The diffuse nucleon spectrum of normalization D as defined in section IV. The true cut-off is less well defined than the cut-off here of order 4×10^{19}ev based upon a 144 il. input for $q(E_c,E)$ for $\gamma_i=2.0$.

Fig.(12) The Haverah Park data (not including the most recently reported events of the 18th ICRC, and dropping the least statistically significant bins at 1.3×10^{20}ev and 2×10^{20}ev corresponding to log()=.13±.5 and log()=.47±.6 respectively). Also shown are our three best fits. The dip is seen and our fit accomodates the ankle structure (with the exception of these highest bins).

Fig.(13) The nucleon anisotropies of our three best fits are compared to

the (large error) data of Haverah Park. The best fit is γ_i=2.0 and seems to agree the best, though the errors are presently too large for this to be meaningful.

Fig.(14) The predicted and fully normalized electron neutrino spectrum for our diffuse+semi-local model fit to the spectrum corresponding to injection index of 2.0. Note the occurance of a neutrino anisotropy above7×10^{18}ev, which is a much smaller effect than the nucleon anisotropy which begins at $\sim10^{18}$ev due to the relatively large diffuse contribution here. The slope is 3.5 with q_o=1/2, and would differ slightly for other values. This spectrum is differential.

TABLE CAPTIONS

Table (I): The "kinematic" quantities pertaining to a given injection slope γ_i. We give (i) D, the normalization of D(E) above 10^{18}ev computed numerically (ii) $c(\gamma_i, 10^{18}\text{ev})$, the neutrino yield at infinite range (iii) $\mathcal{E}(\gamma_i)$, the "differential neutrino yield" defined in eq.(71) (iv) f, the fraction of neutrinos produced by 3 il. to those produced at infinity (v) the requisite bright phase index to fit the observed γ_{obs}=3.0 for q_o=1/2 for given γ_i.

Table (II) The results of two-component model fits to the HP spectrum data: Ω_{diff} is the coefficient of the diffuse component of the differential spectrum in units of $I_N(10^{18}\text{ev})/(10^{18}\text{ev})$ = J. (ii) Ω_{local} is

the semi-local coefficient in units of J. (J so defined is, using HP data, $2.53 \pm .08 \times 10^{-34}/(cm^2\text{-}s\text{-}sr)$) (iii) $\omega = \Omega_D/\Omega_V$ (iv) R_{IC} is the effective diffuse source separation in $(Mpc) \times h_o^{-1/3}$ as obtained from the fit (v) χ^2_E is for the given fit including data above E; (vi) $I_{\nu_e}(E)$ is the integrated neutrino yield above E for the fit.

References

1. K. Greisen, Phys.Rev.Letters, 16,748 (1966)

2. V.A. Kuzmin, G.T. Zatsepin, Zh.Eksp.Teor.Fiz., 4, 78 (1966)

3. V.L. Ginzburg, S.I. Syrovatskii, "The Origin of Cosmic Rays" Oxford, Pergamon (1964)

4. See the useful review of J. Linsley in "Origin of Cosmic Rays" 53-68, ed. Setti, et. al., (1981) and refs. therein. Also, A.M. Hillas, Phys. Reports, 20C, 59 (1975)

5. J. Lloyd-Evans, A.Watson, 8th European Cosmic Ray Symposium, ed. Lucci et. al., Bologna, pp.81-97 (1983)

6. K.O. Theilheim, W. Langhoff, J.Phys. A, 1, 694 (1968); S. Karakula et. al., J. Phys. A, 5, 904 (1972)

7. A.M. Hillas, Canadian Journal of Physics, 46, 5623 (1968)

8. M. Giler, J.Wdowczyk, A.Wolfendale, J.Phys.G; Nucl.Phys., 6,1561 (1980) A. Strong, J. Wdowczyk, A. Wolfendale, J. Phys. A, Math, Nucl., & General 7, 120 (1974) and ibid. 7, 1767 (1974)

9. G. Blumenthal, Phys. Rev. D1, 1596, (1970); see also E. Feenberg and H. Primakoff, Phys. Rev. 73, 449 (1948)

10. J. Lloyd-Evans, A.Pollock, A.Watson, Proc. 16th Int. Conf. on Cosmic Rays, Kyoto, 13,130 (1979)

11. see S. Colgate, contribution to 18th Intl. Cosmic Ray Conf., Bangalore, India (1983)

12. J. Puget et.al. Ap.J., 205, 638 (1976)

13. S.N. Ganguli, B.V. Sreekantun, J. Math A: Math Gen., Vol. 9 No.2, (1976) and F.W. Stecker, Astro. and Space Sci., 20, 47 (1973)

14. S.A. Bonometto, Il Nuovo Cimento Lett. 1, 677, (1971) note the interesting possibility of γ-cascades here.

15. J. Linsley, Proc. of 13th ICRC (Denver) 5, 3207 (1973) and Proc. of 14th ICRC (Munich) 2, 598 (1975) also, most recently: Proc. 18th ICRC (Rapprteur talk, UNM preprint (1983))

16. The Haverah Park Collaboration: (a) G. Cunningham et.al., Astro. J., 236, L71 (1980); (b) G. Brooke et.al. Proc. 16th

ICRC (Kyoto), 8 (1979); J. Phys. A, Math Gen., Vol. 6 (1973), contributions to 18th ICRC (Bangalore) 4, 157 (1983) etc.

17. The Yakutsk group: M.N. Dyankonov, et.al., Proc. 16th ICRC (Kyoto), 8, 168, (1979) D.D. Krasilnikov, et.al. Proc. 18th ICRC (Bangalore) 4, 145 (1983)

18. see L. Horton et.al., Proc. 18th ICRC (Bangalore) 4, 153 (1983) and refs. therein.

19. A.Bower, et.al.,J.Phys.G; Nucl.Phys. 9,L53 (1983)

20. Fly's Eye Experiment: See Proc. 18th ICRC (Bangalore) (1983); for upward moving event limits see B. Cady et.al., Univ. of Utah preprint MN4-15 and P. Sokolsky, Proc. Utah CR Workshop (1983).

21. C.T. Hill, D.N. Schramm, contributions to 18th ICRC (Bangalore) (1983)

22. C.T.Hill, D.N.Schramm, Phys.Lett. 131B, 247 (1983)

23. F. Stecker, Phys.Rev.Letters, 21,1016 (1968) Comments, Astrophys., Vol.7,No.4,pp.129 (1978) The Astrophysics Journal, 228,919 (1979)

24. A. Donnachie, Proc. 1971 Intl' Symp. on Electron Photon Interactions at High Energies, Cornell (1971) also Armstrong et.al., Phys. Rev. D5, 1640 (1972)

25. H. Genzel, W. Pfeil, "Photoproduction Data Below 1.5 Gev", Bonn Univ. PI B1-168, (1972)

26. S. Weinberg, "Gravitation and Cosmology" Wiley & Sons (1972)

27. V. Berezinsky, G.T. Zatsepin, Sov. J. Nucl. Phys., 11, 111 (1970) and V. Berezinsky, V. Ginzburg, L. Ozernoy, cont. to Dumand '80 and '78G F. Stecker in Proc. Neutrino '79, 475 R. Partridge, P.J.E. Peebles, Ap.J. 147, 868 (1967)

28. M. Schmidt, Vol. IX, "Stars & Stellar Systems", G. Kuiper ed., U. of Chicago Press, (1975)

29. M.S. Longair, Monthly Notices, Roy. Astro. Society, 133, 421, (1966)

30. C.T. Hill in proc. of Icoban '84, Park City Utah

31. C.T. Hill and D.N. Schramm, in preparation

32. C.T. Hill, Nucl. Phys. B224, 469 (1983)

33. T. Weiler, UCSD-10P10-233 (1983)

TABLE (I)

γ_i	D	$c(\gamma_i, 10^{18}\,ev)$	$\varepsilon(\gamma_i)$	$f(3;\gamma)$	m
3.0	1.00	2.48×10^{-4}	1.16×10^{-5}	.370	3.5
2.5	1.20	2.17×10^{-3}	1.36×10^{-4}	.399	4.0
2.2	2.20	7.85×10^{-3}	6.13×10^{-4}	.420	4.3
2.0	3.42	1.85×10^{-2}	1.73×10^{-3}	.431	4.5
1.8	5.45	3.86×10^{-2}	4.52×10^{-3}	.468	4.7
1.5	11.46	1.17×10^{-1}	2.19×10^{-2}	.531	5.0

TABLE (II)

γ_i	$\Omega_{diffuse}$	Ω_{local}	ω	R_{IC}	$\chi^2_{(10^{18}ev)}$	$\chi^2_{(5\times10^{18}ev)}$	$I_{\nu_e}(10^{18}ev)$	$I_{\nu_e}(10^{19}ev)$
2.5	.70	.241	2.9	1.73×10^{2}	10.62	10.44	.125	3.9×10^{-4}
2.2	.43	7.15×10^{-2}	5.98	1.36×10^{2}	2.94	2.72	.344	1.09×10^{-3}
2.0	.29	2.04×10^{-2}	14.04	1.02×10^{2}	2.15	1.90	.652	2.06×10^{-3}
1.8	.18	1.22×10^{-2}	14.9	1.00×10^{2}	2.68	1.71	1.07	3.38×10^{-3}
1.5	8.69×10^{-2}	4.04×10^{-3}	21.5	$.88\times10^{2}$	8.44	7.35	2.50	7.91×10^{-3}

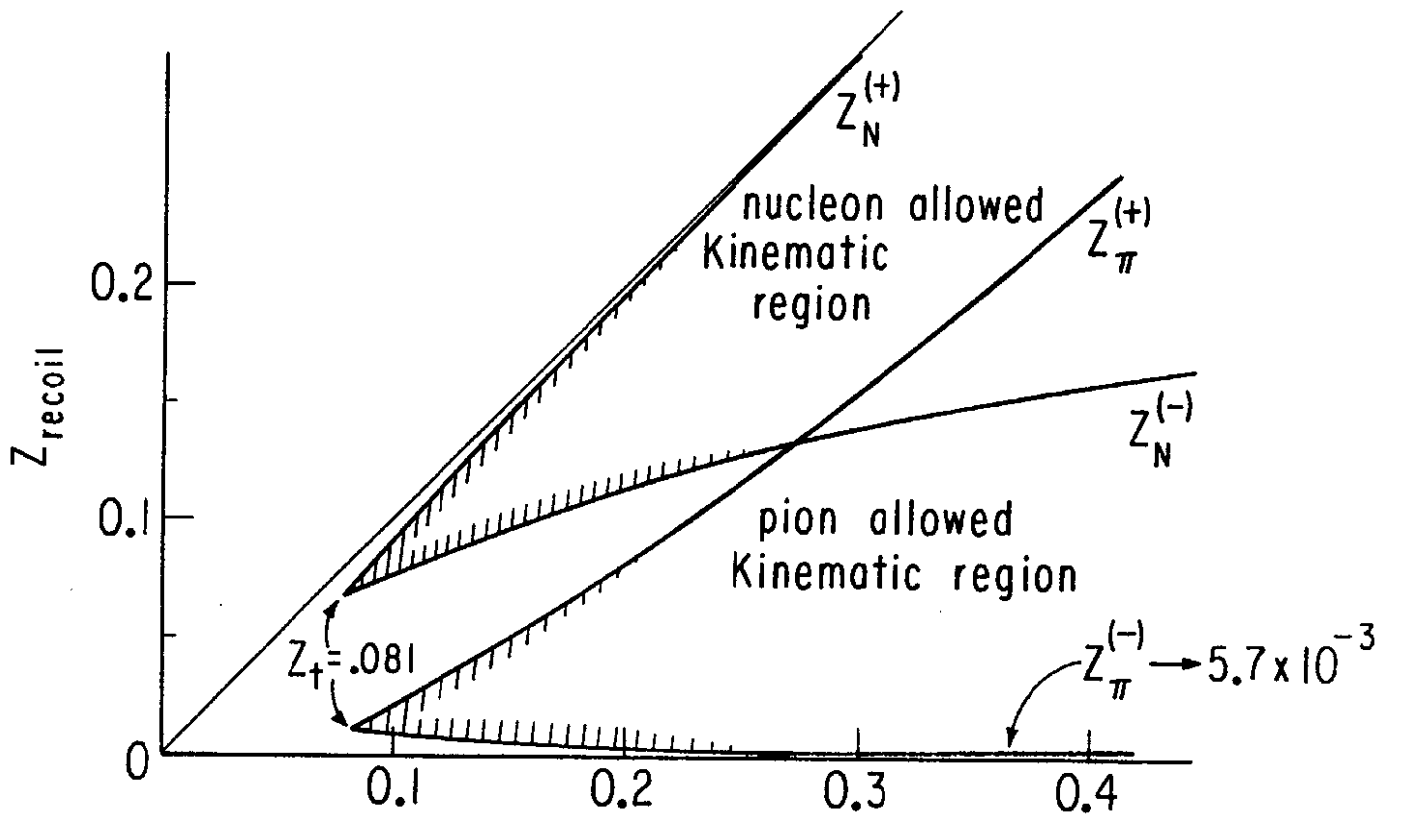
$Z_N^{(+)}$
nucleon allowed
Kinematic
region
$Z_\pi^{(+)}$
$Z_N^{(-)}$
pion allowed
Kinematic region
$Z_t = .081$
$Z_\pi^{(-)} \rightarrow 5.7 \times 10^{-3}$
Z_{recoil}
0.2
0.1
0
0.1
0.2
0.3
0.4

Fig. 1

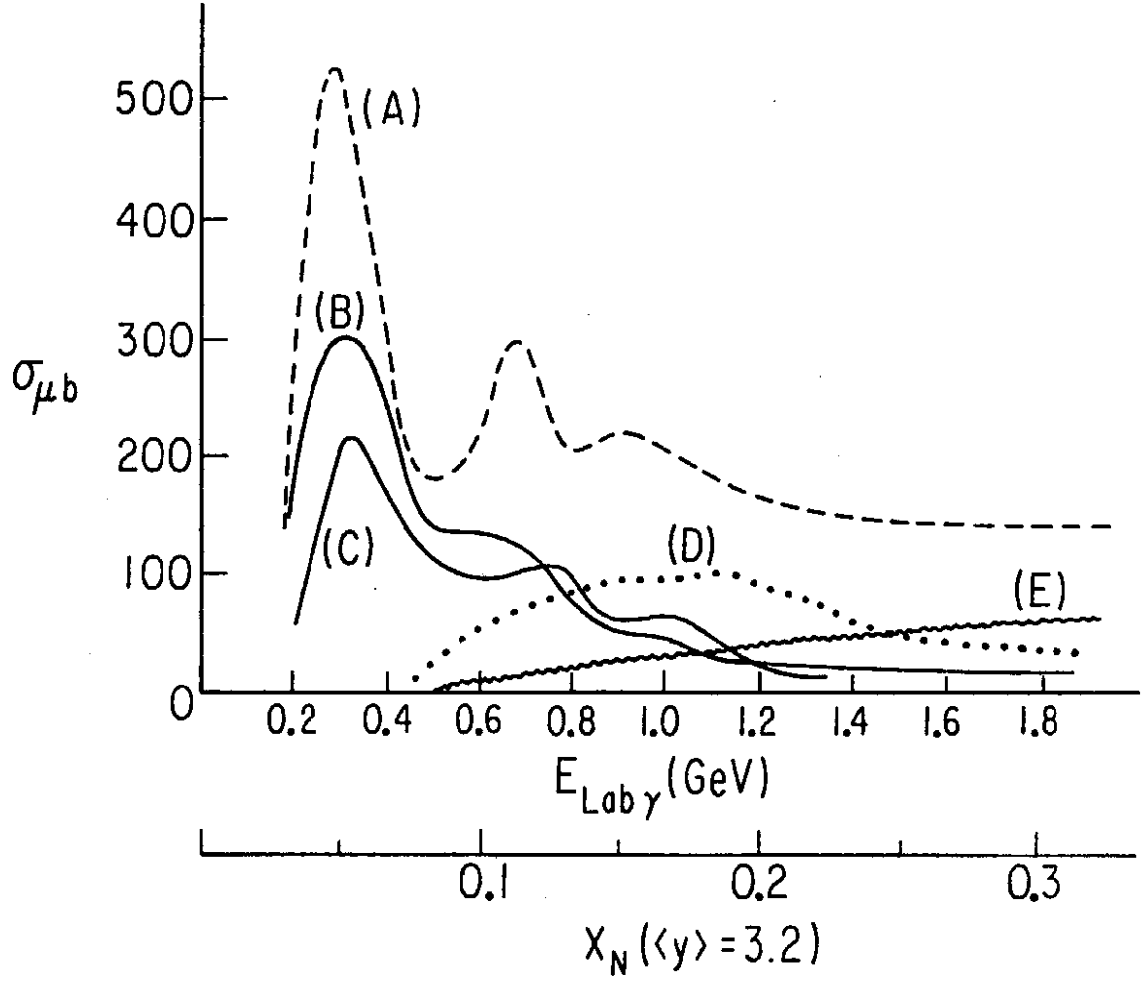
500
400
300
200
100
0
$\sigma_{\mu b}$
(A)
(B)
(C)
(D)
(E)
0.2
0.4
0.6
0.8
1.0
1.2
1.4
1.6
1.8
$E_{Lab\,\gamma}$(GeV)
0.1
0.2
0.3
X_N (⟨y⟩ = 3.2)

Fig. 2

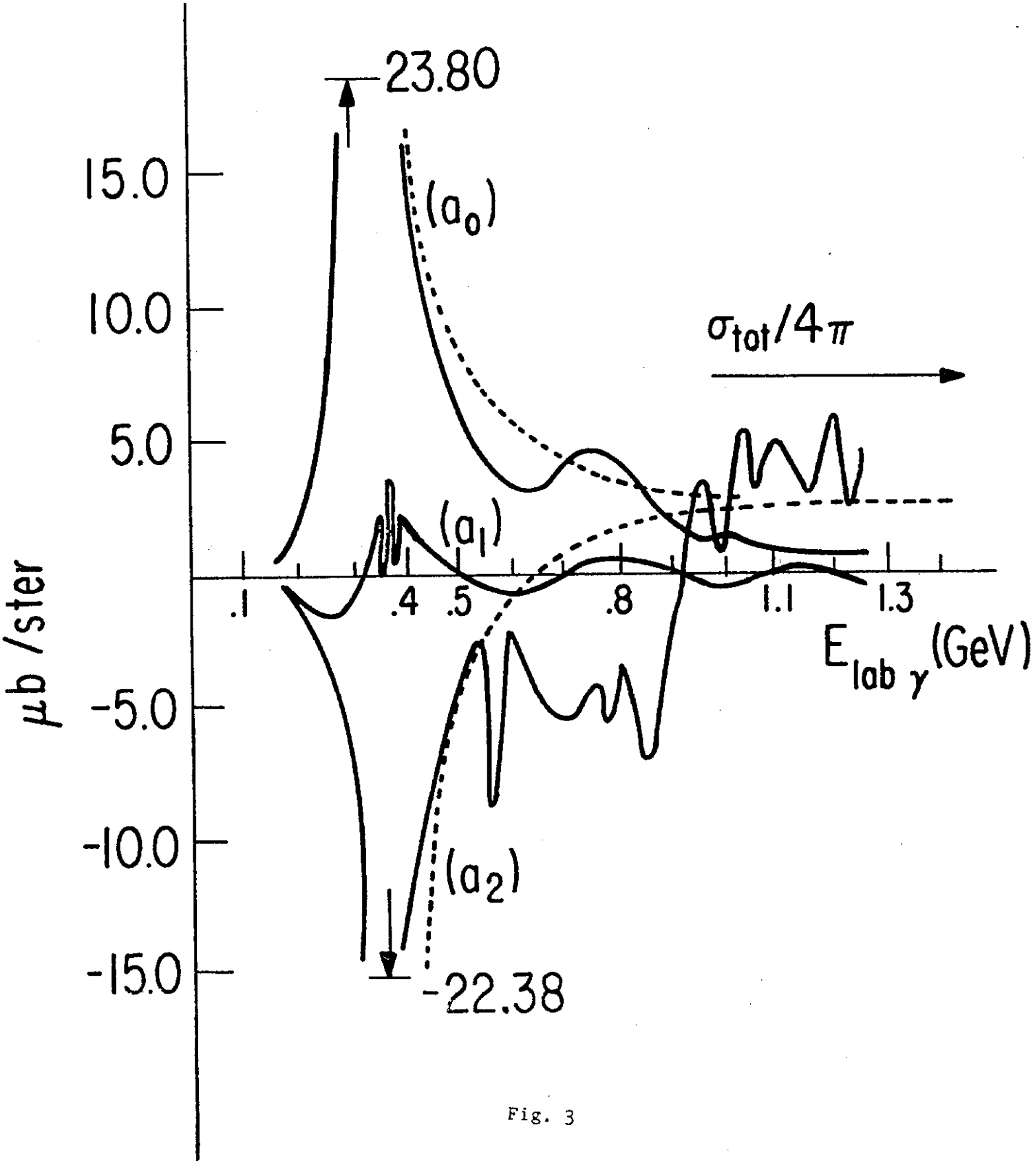
23.80
15.0
10.0
5.0
-5.0
-10.0
-15.0
-22.38
(a_0)
(a_1)
(a_2)
$\sigma_{tot}/4\pi$
.1
.4
.5
.8
1.1
1.3
$E_{lab\ \gamma}$ (GeV)
μb /ster

Fig. 3

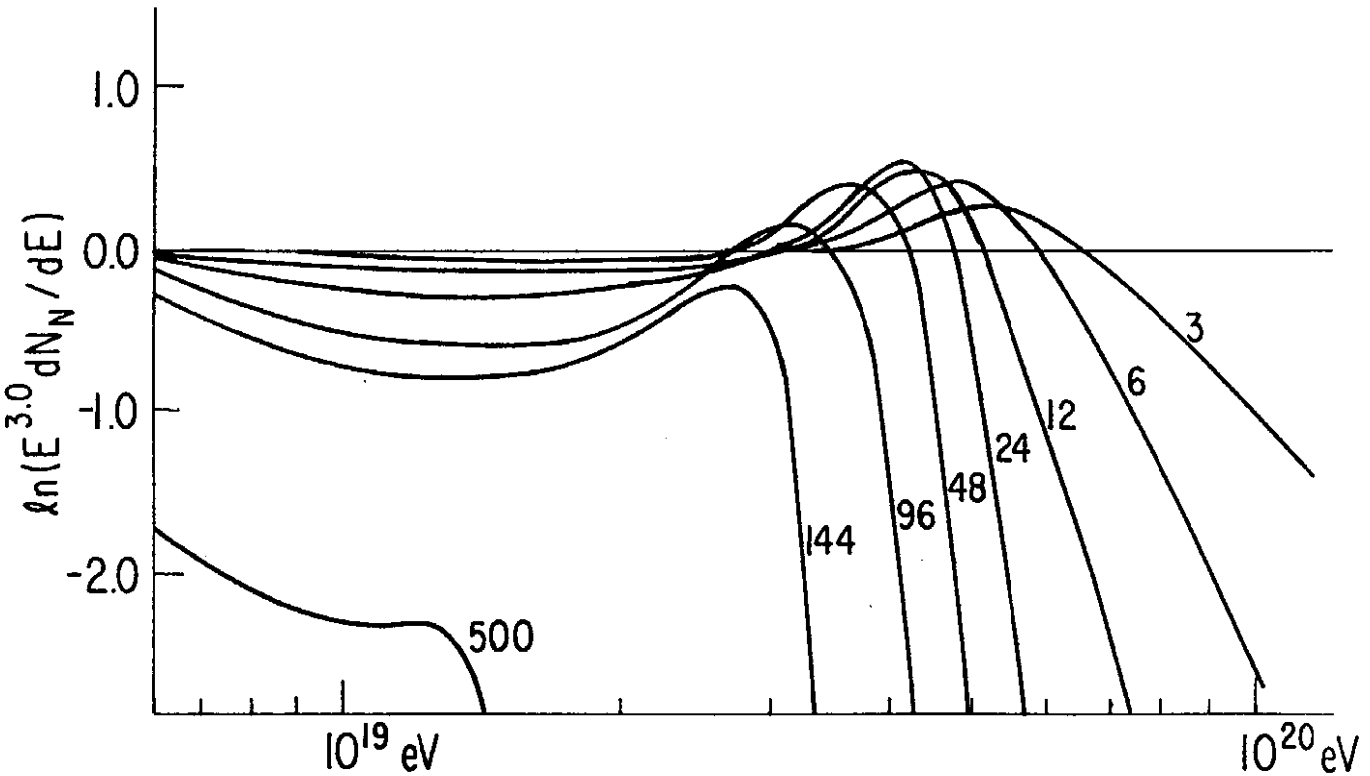

Fig. 4

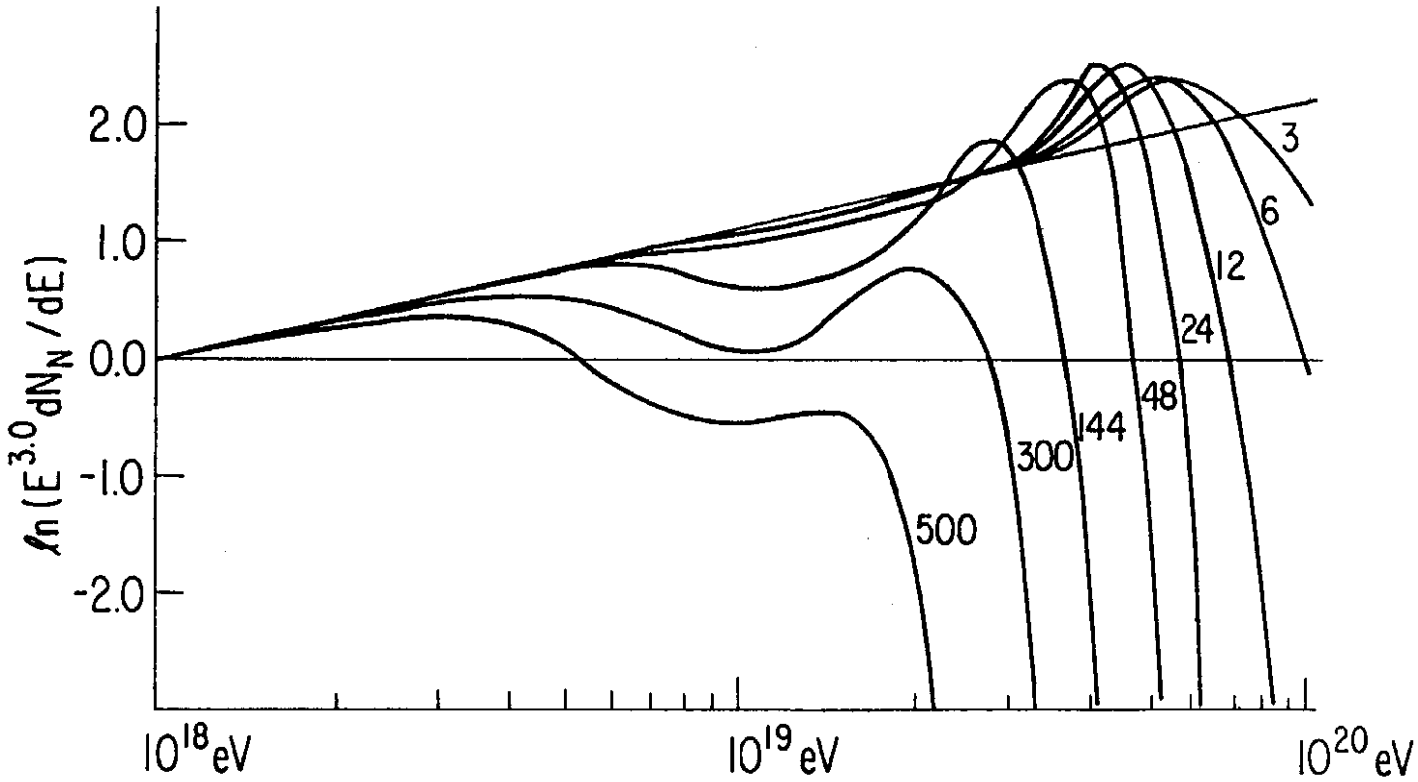
2.0
1.0
0.0
-1.0
-2.0
ℓn(E^3.0 dN_N/dE)
3
6
12
24
48
144
300
500
10^18 eV
10^19 eV
10^20 eV

Fig. 5a

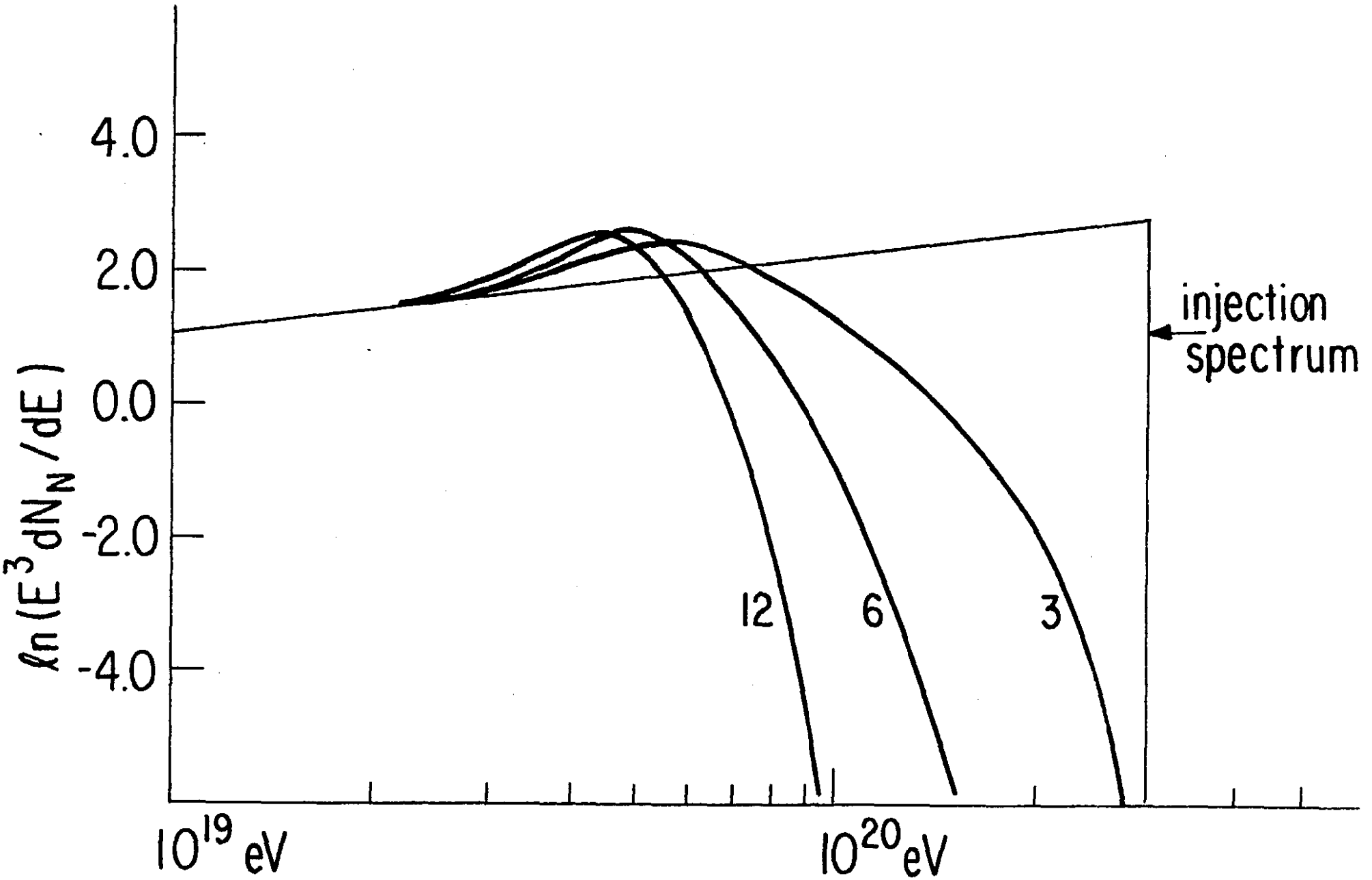
4.0
2.0
0.0
-2.0
-4.0
$\ell n(E^3 dN_N/dE)$
injection spectrum
12
6
3
10^{19} eV
10^{20} eV

Fig. 5b

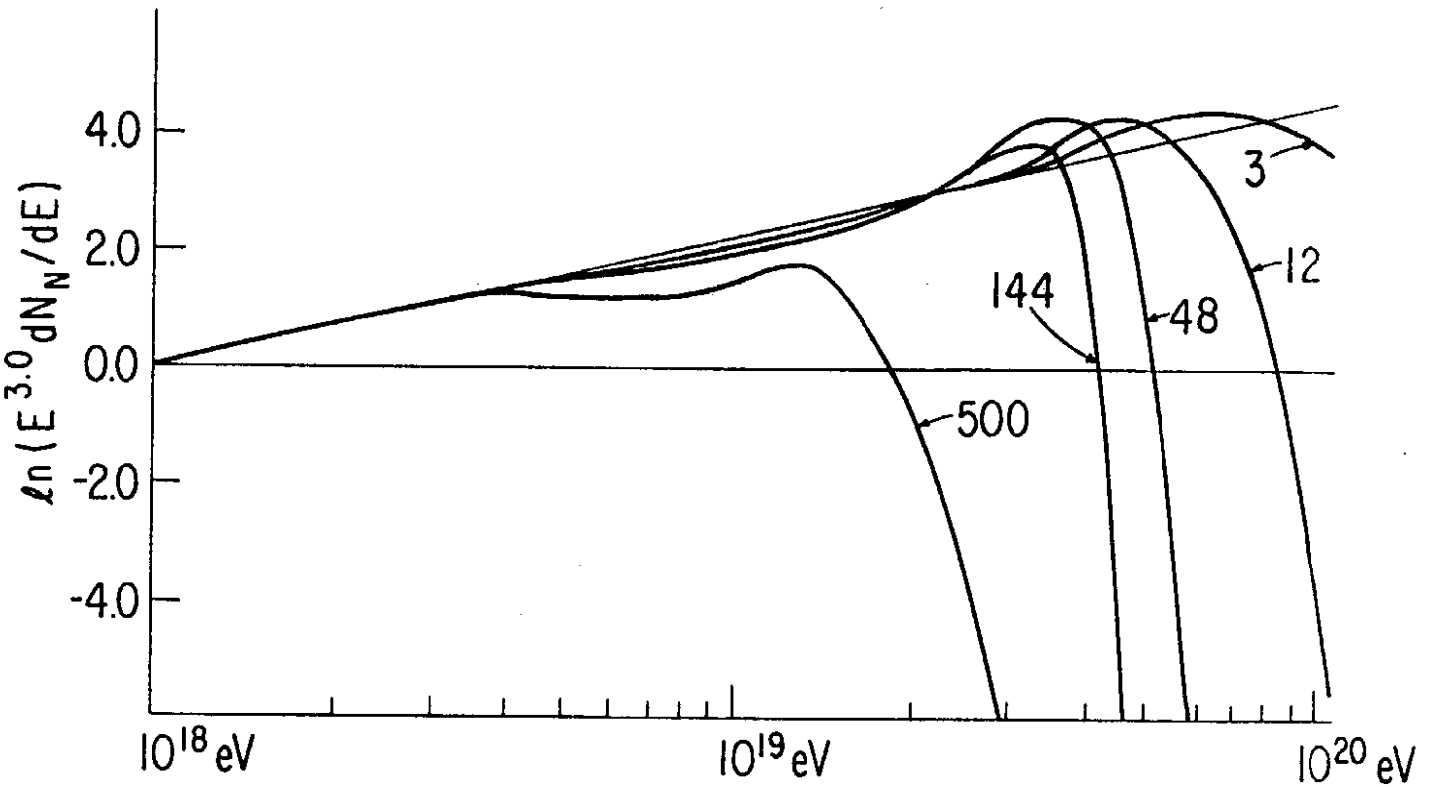

Fig. 6

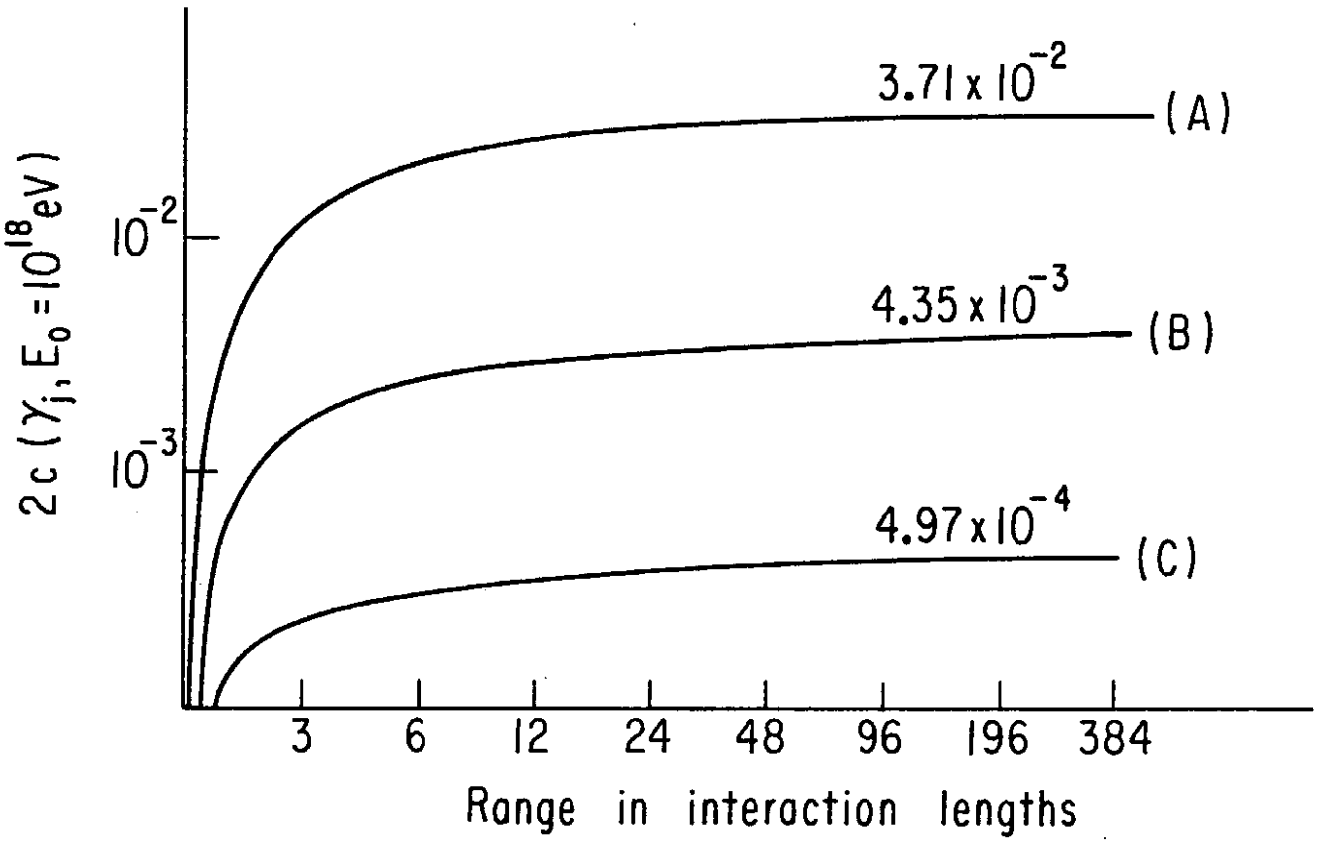
$2c\,(\gamma_j, E_0 = 10^{18} eV)$
10^{-2}
10^{-3}
3.71×10^{-2}
(A)
4.35×10^{-3}
(B)
4.97×10^{-4}
(C)
3
6
12
24
48
96
196
384
Range in interaction lengths

Fig. 7

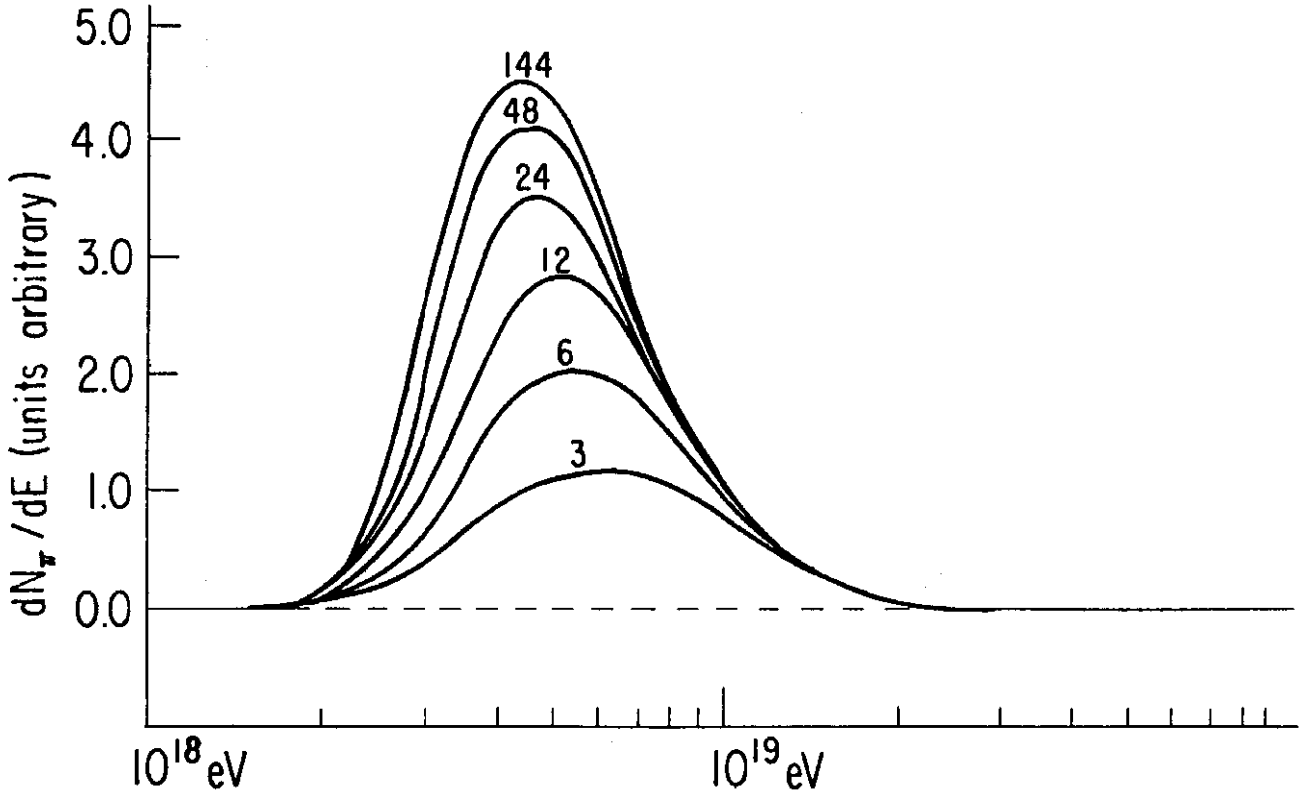
5.0
4.0
3.0
2.0
1.0
0.0
dN_π/dE (units arbitrary)
144
48
24
12
6
3
10^{18}eV
10^{19}eV

Fig. 8a

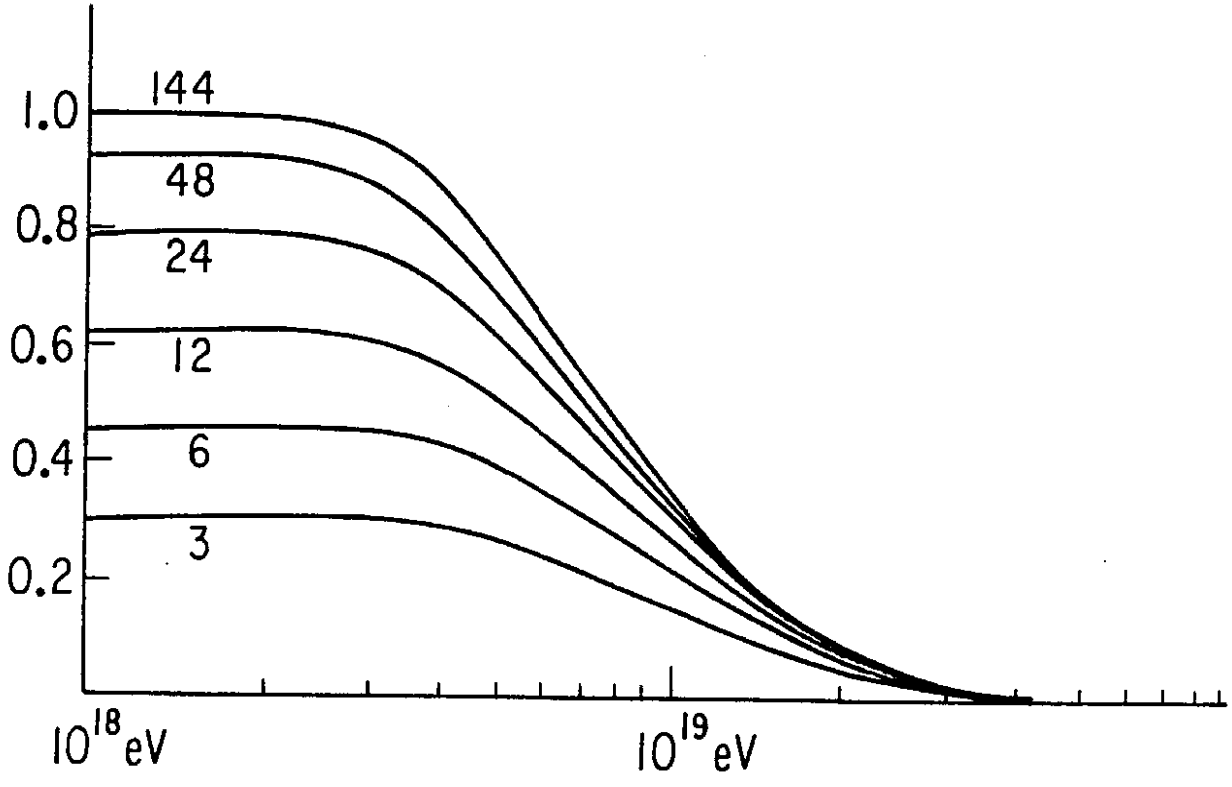

Fig. 8b

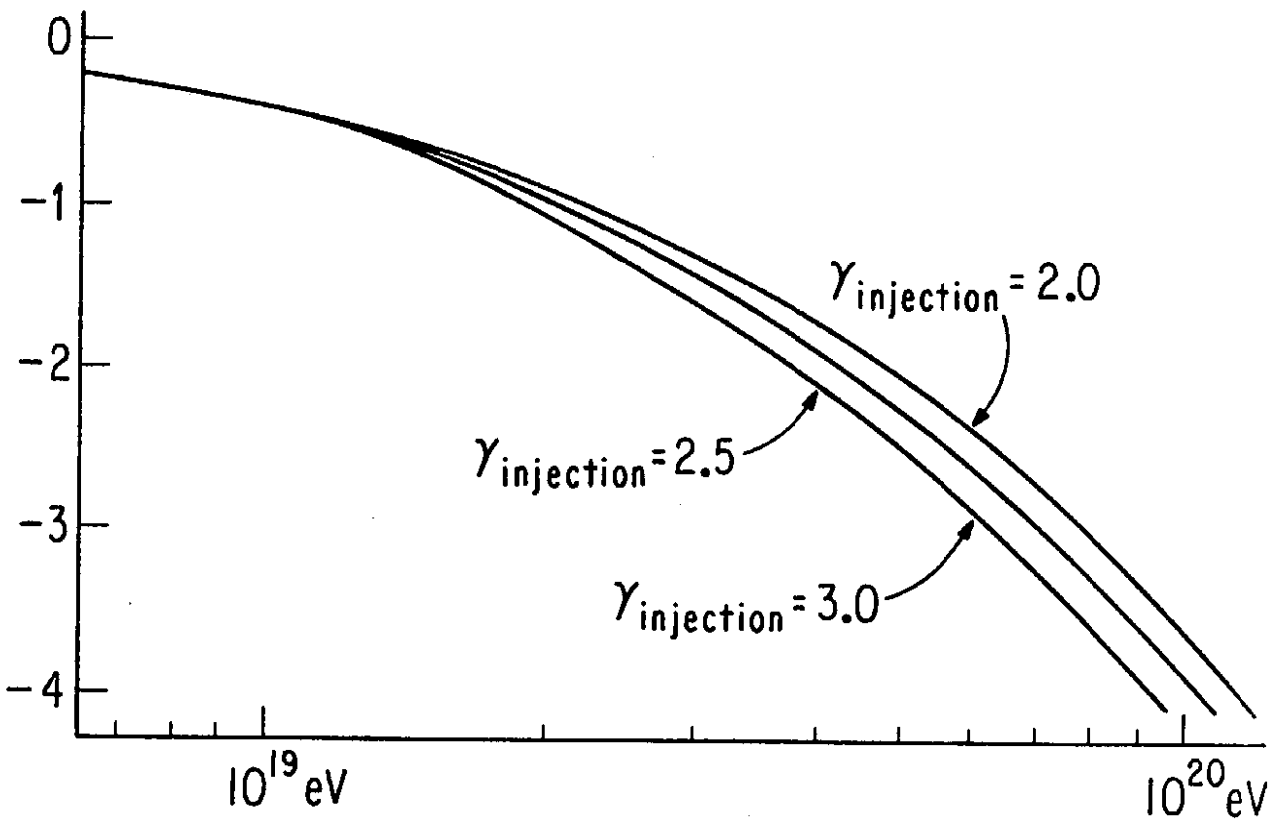
0
-1
-2
-3
-4
$\gamma_{injection} = 2.0$
$\gamma_{injection} = 2.5$
$\gamma_{injection} = 3.0$
10^{19} eV
10^{20} eV

Fig. 9

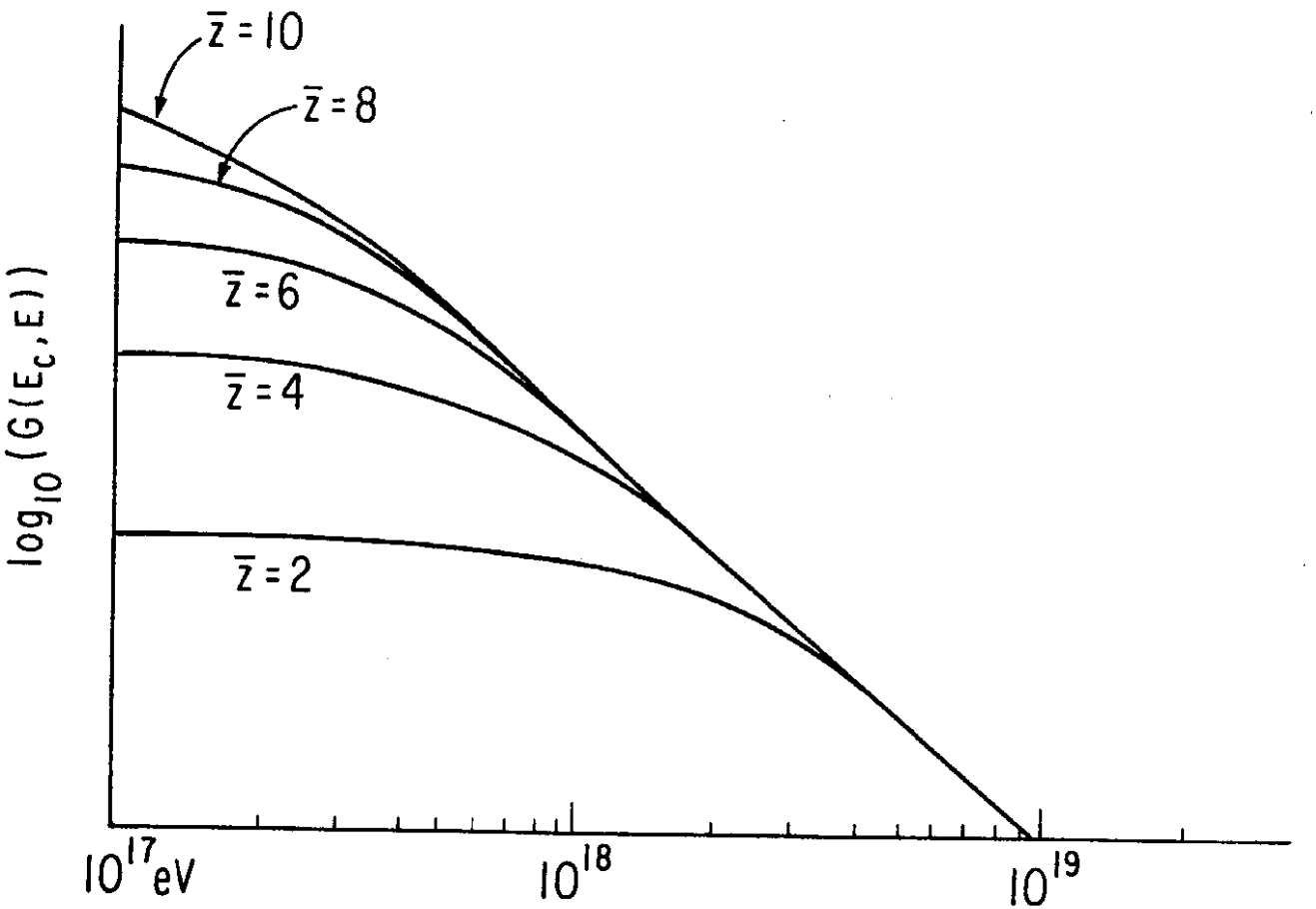

Fig. 10a

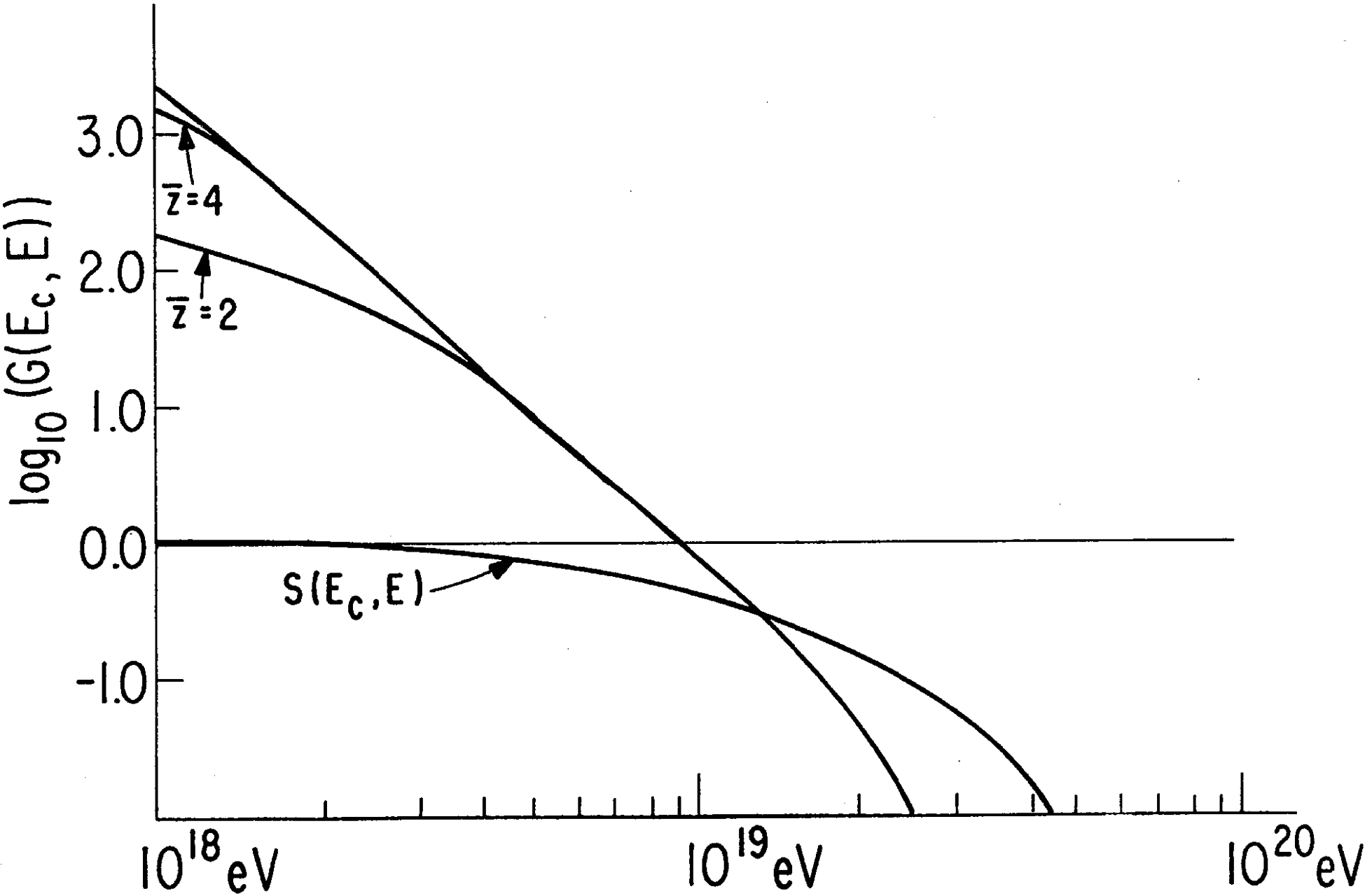
3.0
2.0
1.0
0.0
-1.0
$\log_{10}(G(E_c, E))$
$\bar{z}=4$
$\bar{z}=2$
$S(E_c, E)$
10^{18}eV
10^{19}eV
10^{20}eV

Fig. 10b

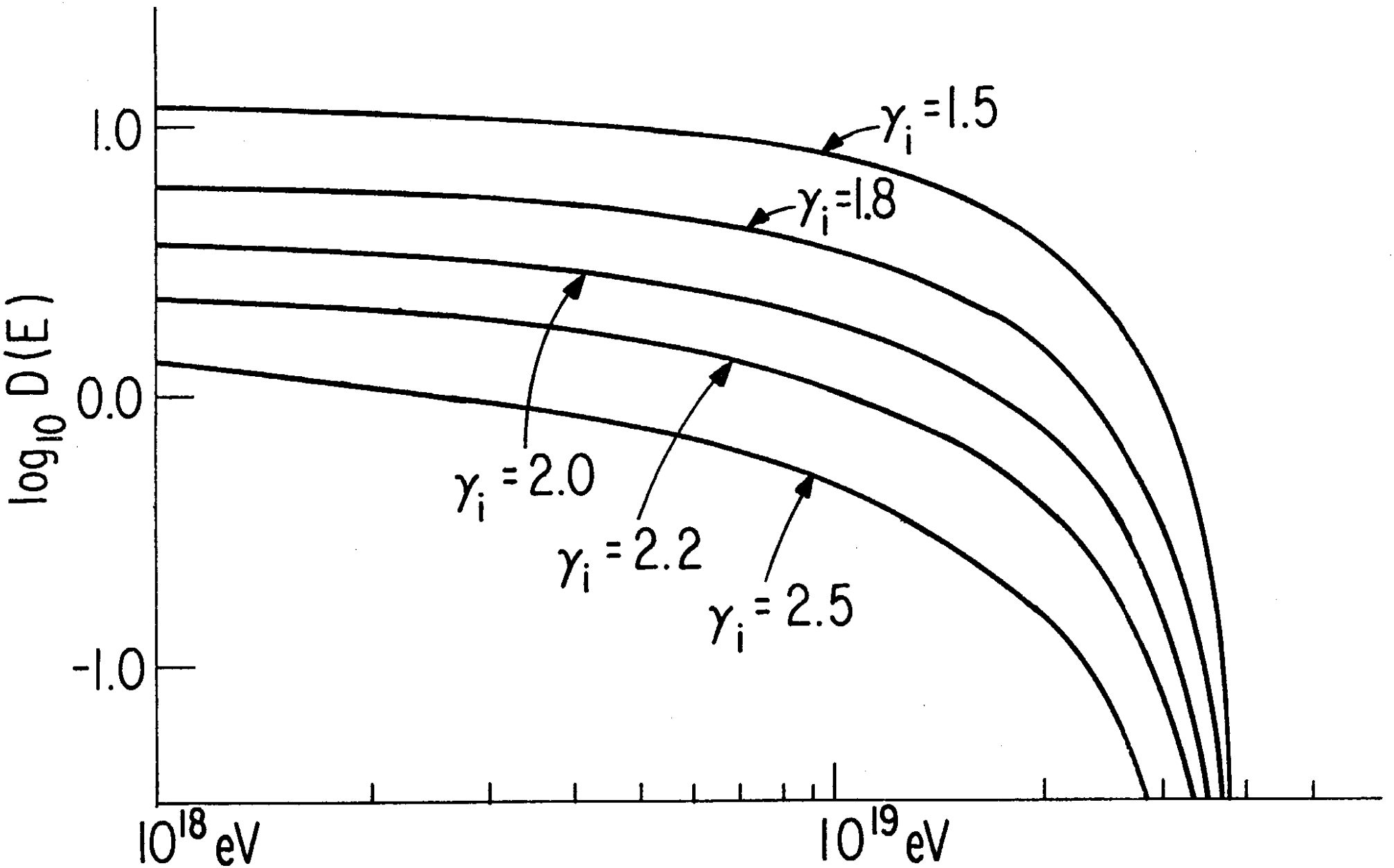
1.0
0.0
-1.0
$\log_{10} D(E)$
$\gamma_i = 1.5$
$\gamma_i = 1.8$
$\gamma_i = 2.0$
$\gamma_i = 2.2$
$\gamma_i = 2.5$
10^{18} eV
10^{19} eV

Fig. 11

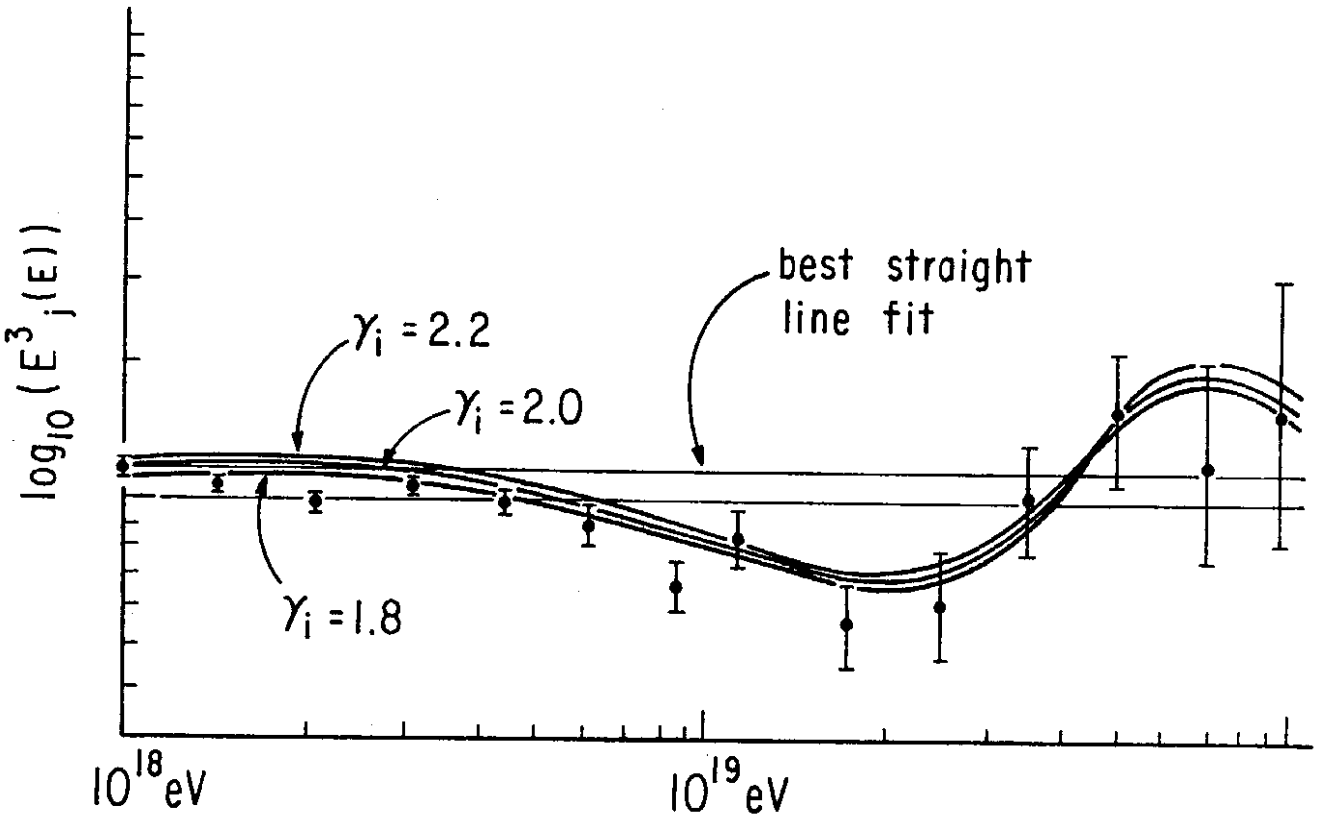
$\log_{10}(E^3_j(E))$
$\gamma_i = 2.2$
$\gamma_i = 2.0$
$\gamma_i = 1.8$
best straight
line fit
10^{18}eV
10^{19}eV

Fig. 12

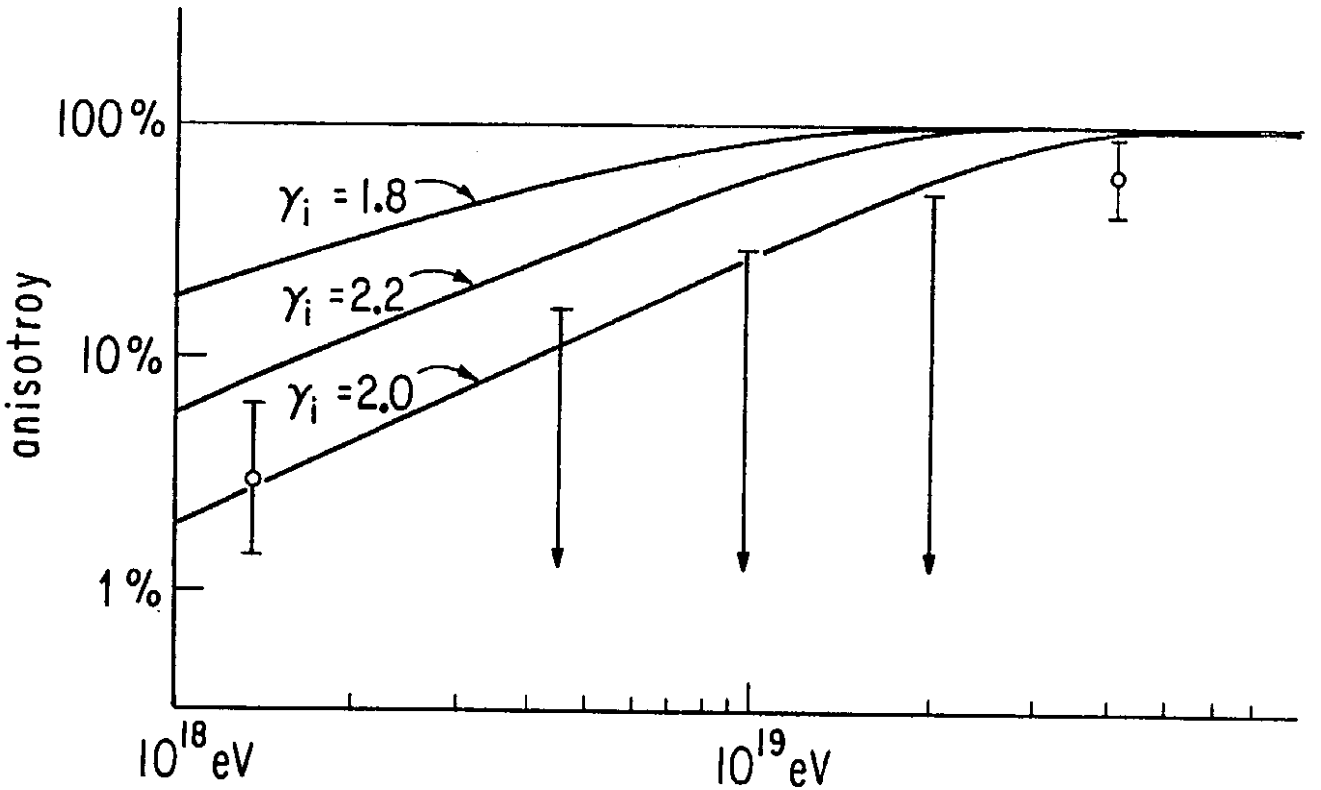
100%
10%
1%
anisotroy
γ_i = 1.8
γ_i =2.2
γ_i =2.0
10^{18}eV
10^{19}eV

Fig. 13

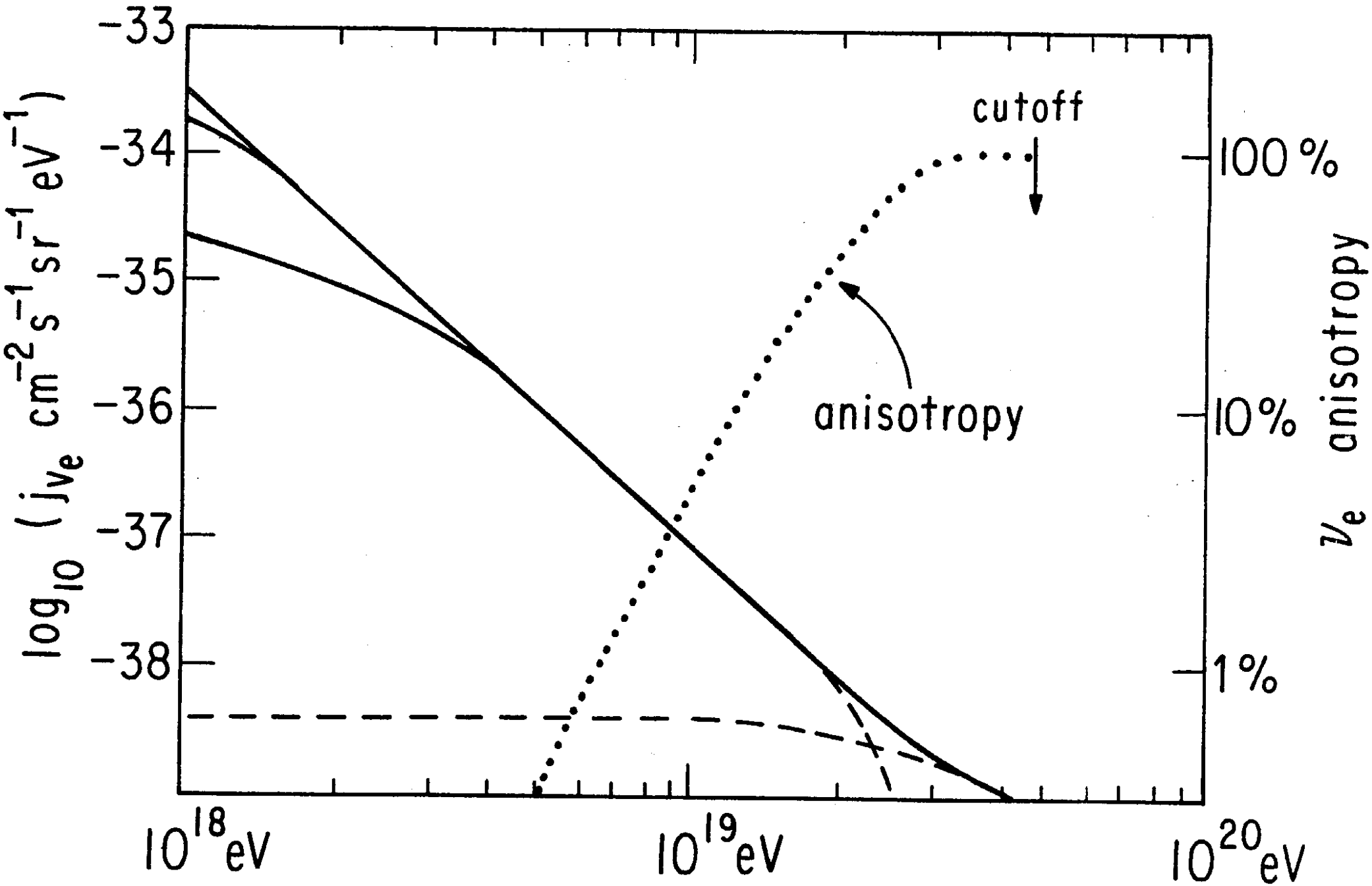
-33
-34
-35
-36
-37
-38
$\log_{10}(j_{\nu_e}\ cm^{-2}s^{-1}sr^{-1}eV^{-1})$
cutoff
anisotropy
100 %
10 %
1 %
γ_e anisotropy
10^{18}eV
10^{19}eV
10^{20}eV

Fig. 14